NOVEL APPARATUS AND TECHNIQUE FOR THE DETERMINATION OF CLATHRATE HYDRATE PHASE EQUILIBRIA

By

VU H.Q. THIEU

A DISSERTATION PRESENTED TO THE GRADUATE SCHOOL OF THE
UNIVERSITY OF FLORIDA IN PARTIAL FULFILLMENT OF THE
REQUIREMENTS FOR THE DEGREE OF
DOCTOR OF PHILOSOPHY

UNIVERSITY OF FLORIDA

1997

To my parents,
my brothers, Anh and Tuyen,
my sister, Hanh,
and to Quyen,
for their everlasting support and encouragement.

ACKNOWLEDGEMENTS

The author wishes to thank all of those who have contributed to his education at the University of Florida. In particular, he extends his greatest thanks to his committee chairman and advisor, Dr. Samuel Colgate. The author considers it an honor to have learned and received support from such an exceptional engineer and chemist.

The author would like to thank Dr. Kathryn Williams for her support and tremendous generosity. This work would not have been possible without the valuable lab space and the unlimited microscope use allowed by her. The author wishes to thank these present and past members of the Colgate research group, Karl Zachary, Dan Tatro, Troy Halvorsen, Johnny Evans and Chadin Dejsupa, for their interactions and encouragement. In particular, the author would like to thank Karl Zachary for his insights on clathrate hydrates chemistry and his lively discussions on the many aspects of graduate research.

The author wishes to acknowledge the technical and moral support of machinist Joe Shalosky, whose expert craftsmanship, patience and understanding greatly contributed to the success of this research. The assistance provided by Lori Clark, particularly the continuous use of her computer, printer and scanner, was greatly appreciated.

Moreover, the author would like to thank members of the Vietnamese Student Organization for their friendships. In particular, Bang Tran, Long Nguyen and Ky Tran have helped make the years at UF memorable ones.

Special gratitude is extended to Quyen Vu for being by the author's side throughout the years in Gainesville. She has made the years in Gainesville the best years of the author's life. Lastly, additional thanks are extended to the author's family for their unending love, understanding and inspiration.

TABLE OF CONTENTS

ACKNOWLEDGEMENTS iii

ABSTRACT vii

CHAPTERS

1 INTRODUCTION 1

2 BACKGROUND 14

Hydrate Structures 14
Guest Molecules of Structures I & II 21
Guest Molecules of Structure H 24
Hydrate Prevention 25
Hydrate Formation and Decomposition 26

3 EXPERIMENTAL 32

Gases & Chemicals 32
Hydrate Cell 33
Interfacing 43
Measurement Hardware 46
    Pressure 46
    Temperature 49

4 EXPERIMENTAL PROCEDURE 53

5 HYDRATE DECOMPOSITION IMAGES 59

6 RESULTS 69

Structure I Hydrates 69
    Methane 69
    Carbon Dioxide 70
Structure H Hydrates of Methane 78
    Methane/Methylcyclohexane 78
    Methane/2-Methylbutane 79
    Discussion 79
Structure H Hydrates of Carbon Dioxide 91
    Carbon Dioxide/Methylcyclohexane 91

Carbon Dioxide/2-Methylbutane 91
Discussion 92
Methane/2,4-Pentanedione 97
Enthalpy of Dissociation (ΔH_d) Determination 103

7 CONCLUSION AND RECOMMENDATIONS 109

APPENDICES

A COMPUTER PROGRAMS 112

B ICE FORMATION 117

C TEMPERATURE CONTROL 119

REFERENCES 125

BIOGRAPHICAL SKETCH 129

Abstract of Dissertation Presented to the Graduate School of
the University of Florida in Partial Fulfillment of the
Requirements for the Degree of Doctor of Philosophy

NOVEL APPARATUS AND TECHNIQUE FOR THE DETERMINATION OF CLATHRATE HYDRATE PHASE EQUILIBRIA

By

Vu H.Q. Thieu

May 1997

Chairperson: Dr. Samuel O. Colgate
Major Department: Chemistry

A novel high-pressure visual cell was developed for the determination of clathrate hydrate phase equilibria. Experimentally, the compact hydrate apparatus was placed on the stage of an optical microscope for observation during warming runs to determine the hydrates' decomposition temperatures and pressures. The microscope enabled close visual examination and video recording of the hydrate cell's contents as it was heated. The onset of hydrate decomposition was noted by the initial formation of microscopic gas bubbles. These grew in size and increased in number as the decomposition temperature was reached and exceeded. Bubble formation at this level has not been previously reported by other researchers.

Some interesting behavior was noted on runs involving structure H hydrate-forming systems, corroborating the proposed concept of transition from structure I to structure H upon hydrate decomposition that was recently reported in the literature. The research examined various hydrate-forming systems involving methane and carbon dioxide, although the method developed can be used with any system of interest.

CHAPTER 1
INTRODUCTION

Clathrate hydrates are inclusion compounds that form when water and certain dissolved gases combine at high pressures and low temperatures. Hydrates are crystalline, non-stoichiometric compounds; the number of gas molecules per water molecule in the hydrate phase is determined by the pressure and temperature conditions at which they form. Water molecules interact strongly by hydrogen bonding, which promotes systematic organization among the assembly of molecules. In the presence of dissolved gas molecules of appropriate size and concentration, three-dimensional hydrogen bonded lattices with large cavities can form. Gas molecules (guests) with molecular dimensions smaller than those of the lattice cavities can occupy them, and the occupation of these cavities results in the stabilization of the lattice through van der Waals' forces. At elevated pressures, gas hydrates can form in natural and artificial environments at temperatures above and below the normal freezing point of water. Natural gas components such as CH_4, C_2H_6, C_3H_8, H_2S are known to form gas hydrates in nature and in gas production pipes. Other gases including Ne, Ar, Xe, N_2, and O_2 have been shown in the laboratory to form hydrates as well.

The first known clathrate hydrate was discovered by Sir Humphrey Davy in 1810. He found that a solid could be formed when an aqueous solution of chlorine was cooled below 9.0 °C.[1] Faraday later confirmed the existence of such a solid compound and suggested that its composition was nearly one part of chlorine to ten parts of water.[2] It is now known that over 100 species can combine with water to form such non-stoichiometric solids. These solids are often referred to as gas hydrates, although a more descriptive and hence preferred designation is clathrate hydrates.

Clathrate hydrates became more than a laboratory curiosity in the early 1930s. At that time, the oil and gas industry in the United States was growing rapidly, and it was then that the natural gas and petroleum industry first encountered problems with transmission lines being blocked by some strange ice-like formation, often at temperatures above the normal freezing point of water. Hammerschmidt[3] later determined that the plugging of natural gas pipelines was not caused by ice formation but by the formation of clathrate hydrates. This discovery led to a more practical interest in gas hydrates, in which the prevention of hydrate formation became a major concern to the industry and led to a large number of studies of the phase behavior of hydrate-forming systems.

Over the 125 years following their discovery, workers in the clathrate hydrates field concentrated on two areas of research. The first focus was on identifying all the species that could form gas hydrates and the pressure-temperature conditions at which the formation occurs. Secondly, researchers wanted to describe these species quantitatively; their compositions, structures, and physical properties. A timetable summary of the research done over that period was published by Sloan.[4]

Recently, Sloan and other workers in the field suggested that hydrates in nature are far more ubiquitous than previously suspected, with a good probability of occurrence wherever methane and water are in close proximity at low temperatures and elevated pressures. Clathrate hydrates are naturally of interest to pure science, but there are practical reasons for the need to know and understand more about them as well. Significant among these are the following:

a) Clathrate hydrates represent a source of problems in the natural gas and petroleum industry because the conditions at which oil and gas are produced, transported, and processed are often suitable for clathrate hydrate formation.

b) Vast resources of naturally occurring hydrates are known to exist in underground deposits.

Estimates based on reliable geological surveys suggest that the total amount of oxidizable carbon trapped in natural gas hydrates on Earth may surpass the energy content of the total conventional fossil fuel reserves by as much as a factor of two.[5-6] Thus, naturally occurring clathrate hydrates, containing mostly methane, are being considered as a potential future source of energy.

c) Since clathrate hydrates reside in relative close proximity to the atmosphere, they represent a huge reservoir of greenhouse gases and a potential source of global warming from methane release into the atmosphere.

Figure 1-1 shows the locations of known and inferred hydrate deposits throughout the world. The dark circles and dark squares indicate hydrate deposits in subsea beds and in permafrost regions, respectively.

While a great deal of hydrate research has been performed in the last half century, the accumulation of new knowledge on the physical and chemical properties of natural gas hydrates and the advancement of techniques for their determination has been impeded by the difficulties which often attend measurements at hydrate-forming conditions. Measurements of the temperature, pressure, and composition are necessary for the determination of hydrate formation or decomposition conditions. In Figure 1-2, a partial phase diagram for the methane-water system is shown. The region to the left of the equilibrium line represents the methane hydrate region, whereas the region to the right represents the two-phase region of methane gas and the water rich phase.

Experiments to determine the phase equilibrium behavior of any hydrate-forming system typically involve the use of PVT (pressure, volume, temperature) cells where changes in pressure are monitored while the cell is heated or cooled under isochoric conditions. The onset of hydrate formation is noted by a drop in pressure (or a pressure increase in the case of hydrate decomposition). Figure 1-3 shows a simplified experimental set-up where water is charged with propane gas in a vessel. Hydrate crystals, in general, tend to grow near the gas-liquid interface. Observations of the temperature and pressure and their changes reveal the conditions at which the hydrate crystals form and dissociate.

Another apparatus for hydrate formation is shown in Figure 1-4. The vessel in this apparatus contains stainless steel bearing balls which, when agitated, serve to mix the gas-water sample and thus facilitate rapid hydrate growth. In this set-up, the temperature of the cell is held constant while the reaction chamber is vigorously shaken. Hydrate

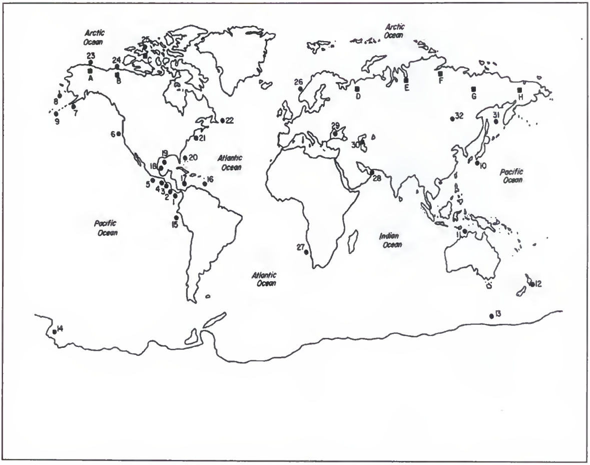

Figure 1-1. Locations of known and inferred hydrate deposits.[5]

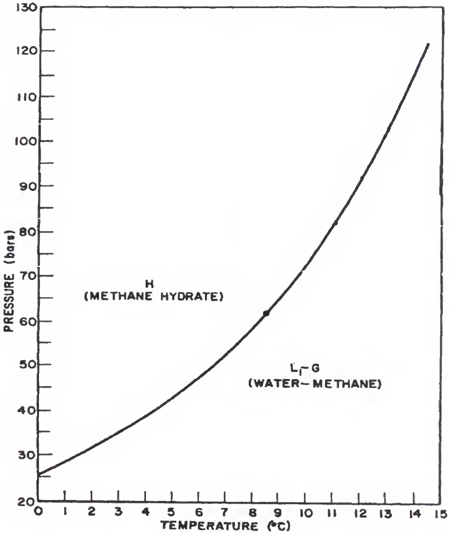

Figure 1-2. Three phase equilibrium line for hydrate-liquid water-methane gas.[7]

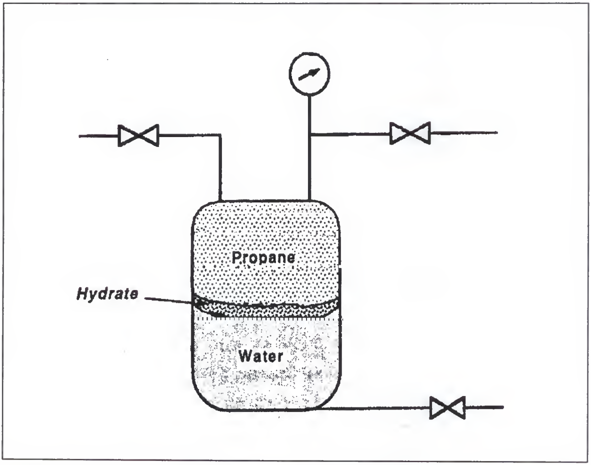

Figure 1-3. Apparatus for the simulation of hydrate formation in the laboratory.[8]

formation is determined to be the point at which a catastrophic drop in pressure occurred.

A recent approach to the experimental study of hydrate phase equilibria is illustrated in Figure 1-5. The experimental apparatus shown consists of a Jerguson sight glass cell rocked about its axis. Hydrate growth or decomposition inside the cell could be visually observed through the window opening in the cell. In this manner, visual information along with temperature and pressure data aided in the determination of hydrate phase equilibria.

Studies by each of these methods have revealed the extreme hysteresis and metastability[11] inherent in hydrate-forming systems. This behavior complicates the task of comparing results from different laboratories. Moreover, to obtain any results in conventional PVT systems such as those described above, a relatively large quantity of hydrate must be formed or decomposed in order to give a sufficiently strong signal for detection.

Figure 1-6 shows the hysteresis effect in a typical hydrate experiment as an isochoric pressure trace of the hydrate formation and hydrate decomposition cycles. Initially, cooling of a hydrate cell is required for hydrate formation. The letter O on the plot indicates the start of hydrate formation which was accompanied by a sharp drop in system pressure. With each successive cooling run made on the same sample, the temperature at which hydrate formation

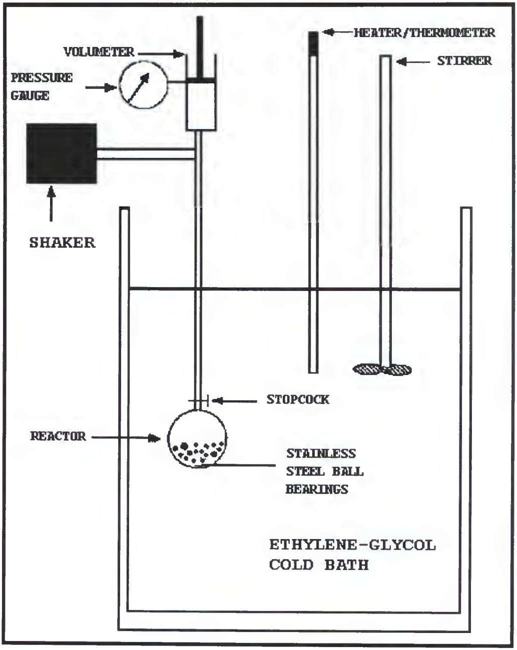

Figure 1-4. Apparatus for hydrate formation with mixing mechanism.[9]

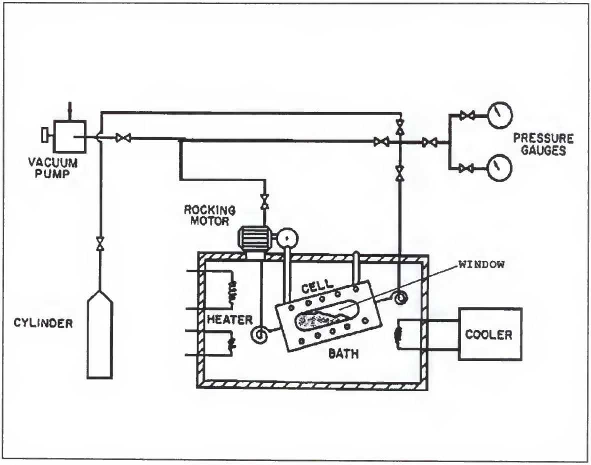

Figure 1-5. Apparatus for hydrate formation with a window for visual observations.[10]

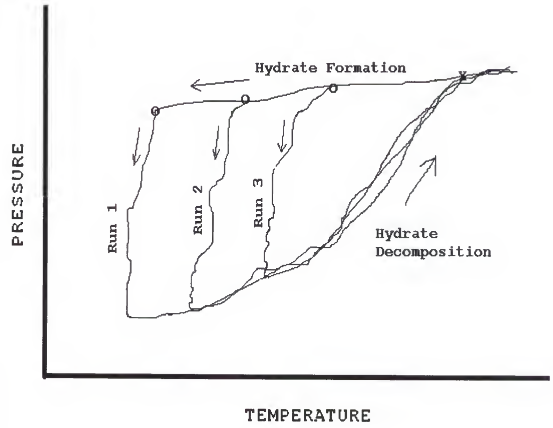

Figure 1-6. Plot of pressure versus temperature for a typical hydrate formation experiment, showing the hysteresis effect.

begins is higher than the previous trial. All three runs follow a similar path upon heating as shown with the hydrate decomposition curve. Point X indicates the conditions at which hydrate decomposition is complete for all runs. Thus, in the determination of phase equilibria of hydrate-forming systems, observations should be made while heating the cell to take advantage of the absence of water memory effects which occur during hydrate decomposition.

In view of this background, the focus of this work was concentrated in three areas: 1) the development of a hydrate cell capable of stimulating hydrate growth and decomposition under appropriate temperatures and pressures, 2) the determination of phase equilibria conditions of various hydrate-forming systems and 3) the creation and utilization of a microscopic cell capable of yielding definite visual confirmation of hydrate decomposition along with temperature and pressure information.

The research plan was to study the phase equilibria behavior of several clathrate hydrate systems. The temperature and pressure ranges of interest are from 273 K to 288 K (0 °C to 15 °C) and from 1.3 MPa to 7.0 MPa (200 psi to 1,000 psi). The apparatus works with small samples and enables the visual determination of the onset of hydrate growth and, more importantly, hydrate decomposition using a microscope.

CHAPTER 2
BACKGROUND

Hydrate Structures

Two distinct families of gas hydrates, designated as structure I[12] (SI) and structure II[13] (SII), have been identified, mainly through X-ray diffraction studies in the early 1950s. Structure I and structure II hydrates are the most common hydrate structures and can be formed by water and light hydrocarbon molecules (methane to butane), and by other small, volatile species such as hydrogen sulfide, carbon dioxide, and nitrogen. SI hydrates are typically found *in situ* in deep oceans with biogenic gases such as methane, carbon dioxide and hydrogen sulfide. SII hydrates are formed predominantly in natural gas pipelines due to the presence of molecules such as propane and butane.

The hydrogen bond principally dictates and promotes the interaction of water molecules, favoring bonding in tetrahedral structures similar to that of ice. Cells with pentagonal faces formed through hydrogen bonding are fundamental to the entire water-based solid framework. Hydrate structures normally form from repeated assemblies of these crystal structures, containing a basic "building block" water cavity referred to as the 5^{12} cavity. The 5^{12}

abbreviation denotes a pentagonal dodecahedron with 12 pentagonal faces.

Structure I hydrates are formed by the linking of the vertices of these 5^{12} cavities with the verticies of large cavities composed of 12 pentagons and 2 hexagons ($5^{12}6^{2}$). The $5^{12}6^{2}$ designation refers to a polyhedron consisting of 12 pentagonal and 2 hexagonal faces. Structure I hydrates belong to the class body-centered cubic crystal lattices. The unit crystal structure of SI has the formula $2M_1 \bullet 6M_2 \bullet 46H_2O$, where M_1 and M_2 are the 5^{12} and $5^{12}6^{2}$ cavities, respectively.

Structure II hydrates are formed from the linking of the faces of the 5^{12} cavities. This linking results in interstices of large cavities with faces composed of 12 pentagons and 4 hexagons ($5^{12}6^{4}$). The $5^{12}6^{4}$ cavities are polyhedra with 12 pentagonal and 4 hexagonal faces. Structure II hydrates belong to the class diamond cubic crystal lattices. The unit crystal structure of SII has the formula $16M_1 \bullet 8M_3 \bullet 136H_2O$, with M_1 and M_3 being the 5^{12} and $5^{12}6^{4}$ cavities, respectively. The cavities found in SI and SII clathrate hydrates are illustrated in Figure 2-1. Figure 2-2 shows the hydrate crystal unit structures of SI and SII.

A new structure, named structure H (SH), was discovered in 1987 based on ^{2}H, ^{129}Xe NMR, X-ray and neutron diffraction studies.[14] The new clathrate was designated "H" since its structure belongs to the hexagonal space group. Structure H

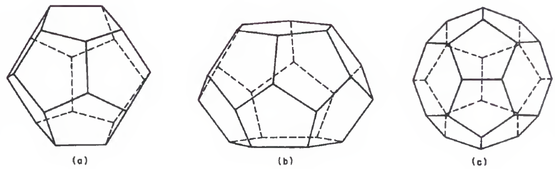

Figure 2-1. Three cavities[4] in clathrate hydrates: (a) 5^{12} (b) $5^{12}6^{2}$ and (c) $5^{12}6^{4}$. Cavities (a) and (b) are common to SI while cavities (a) and (c) are common to SII.

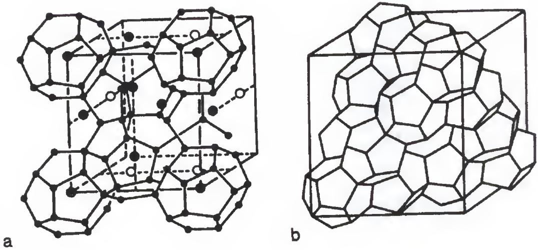

Figure 2-2. Hydrate unit crystal structures: (a) Structure I[12] and (b) Structure II.[13]

hydrates are formed in experimentally stimulated hydrate-forming systems and have yet to be found outside the laboratory. Structure H hydrates appear to contain three cavity types: $4^3 5^6 6^3$, 5^{12} and $5^{12}6^8$. The unit crystal is composed of 34 water molecules and has the formula $2M_1 \bullet 3M_2 \bullet M_3 \bullet 34H_2O$, where M_1, M_2 and M_3 are the $4^3 5^6 6^3$, 5^{12} and $5^{12}6^8$ cavities, respectively. The three cavities along with an orthogonal view of structure H hydrates are shown in Figure 2-3 and Figure 2-4.

The main characteristics of the cavities found in the three hydrate structures are summarized below in Table 2-1. It should be noted that the small cavity of SH hydrates is slightly larger in size than the small cavity common to SI and SII, while the large cavity of the structure H is larger than the large cavities of either structure I and II.

Table 2-1. Cavities present in structures I, II and H.

Cavity Type	5^{12}	$5^{12}6^2$	$5^{12}6^4$	$4^3 5^6 6^3$	$5^{12}6^8$
Cavity Diameter (Å)	4.92	5.76	6.47	5.22	8.53
Cavities/Unit Cell (SI)	2	6	---	---	---
Cavities/Unit Cell (SII)	16	---	8	---	---
Cavities/Unit Cell (SH)	3	---	---	2	1

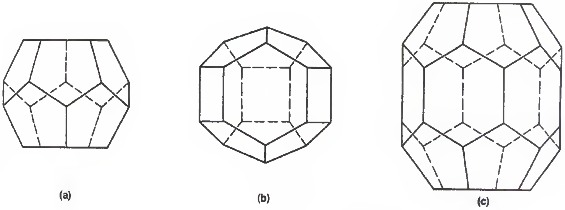

Figure 2-3. Three cavity types[15] in Structure H hydrate: (a) 5^{12} (b) $4^3 5^6 6^3$ and (c) $5^{12} 6^8$.

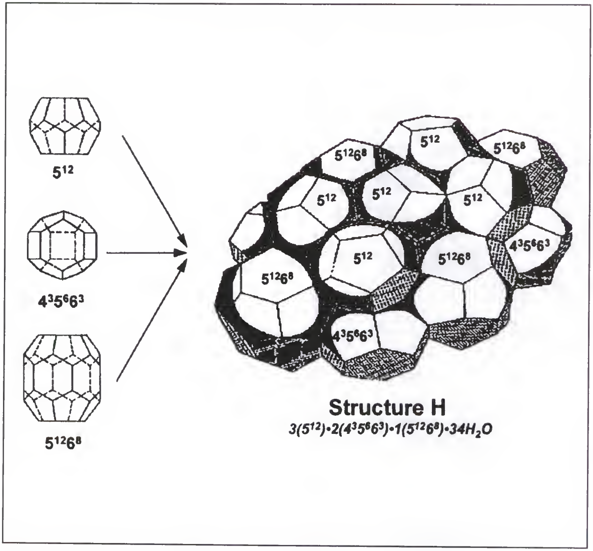

Figure 2-4. Orthogonal view of Structure H.[15]

Guest Molecules of Structures I & II

Typically, guests with molecular diameters smaller than the diameter of a cavity can occupy it, and each cavity can contain at most one guest molecule. Simple gas hydrates, those containing only one type of guest species, are fundamentally important to the understanding of hydrates and thus are the most commonly studied.[4] The molecular diameter of the guest molecule relative to the size of the cage determines which type of hydrate structure it forms. Of the natural gas components which form simple hydrates, methane, ethane, carbon dioxide, and hydrogen sulfide form structure I. Nitrogen, propane and isobutane are known to form structure II hydrates as simple hydrates.

Ratios of guest molecular diameters to cavity diameters for some species that form simple hydrates in structures I and II are shown in Table 2-2. The ratios denoted with a "#" indicate the cavity occupied by the simple hydrate former. Table 2-2 shows a ratio lower bound of about 0.77, below which the molecular attractive forces do not lead cavity stability. Moreover, a guest molecule can not fit into a cavity without distortion if its molecular diameter to cavity diameter ratio is above the upper bound ratio limit of about 1.0. Species such as H_2 and n-C_4H_{10} are not capable of forming known hydrates since they are either too small to stabilize a cavity or too large to fit inside. Consequently, guests capable of entering the 5^{12} cavity of

Table 2-2[*]. Molecular diameter to cavity diameter ratios for some guest molecules.

		Molecular Diameter Cavity Diameter			
		Structure I		Structure II	
	Cavity Type	5^{12}	$5^{12}6^{2}$	5^{12}	$5^{12}6^{4}$
Guest	Diameter (Å)				
H_2	2.72	0.553	0.470	0.555	0.421
Ar	3.8	0.772	0.660	0.775$^{\#}$	0.599$^{\#}$
N_2	4.1	0.833	0.712	0.836$^{\#}$	0.634$^{\#}$
CH_4	4.36	0.886$^{\#}$	0.757$^{\#}$	0.889	0.675
H_2S	4.58	0.931$^{\#}$	0.795$^{\#}$	0.934	0.708
CO_2	5.12	1.041	0.889$^{\#}$	1.044	0.792
C_2H_6	5.5	1.118	0.955$^{\#}$	1.122	0.851
C_3H_8	6.28	1.276	1.090	1.280	0.971$^{\#}$
i-C_4H_{10}	6.5	1.321	1.128	1.325	1.005$^{\#}$
n-C_4H_{10}	7.1	1.443	1.232	1.447	1.098

---

[*] table modified from Sloan[4], p.46.

[#] indicates the cavity occupied by the simple hydrate former.

either structure will also enter the large cavity of that structure.

Of particular interest to the research presented in this work are the gases methane and carbon dioxide. Methane can fit into any of the cavities in SI and SII. It offers the greatest stability to the 5^{12} cavity and very little stability to the $5^{12}6^4$ cavity. The 5^{12} cavity in either structure is almost equally stabilized. However, methane forms SI hydrates because it stabilizes the $5^{12}6^2$ cavity more than the $5^{12}6^4$ cavity. From the ratios presented in Table 2-2, the diameter ratio of methane to the small cavity (5^{12}) of structure I is 0.886 while the diameter ratio of methane to the small cavity (5^{12}) of structure II is 0.889. Methane is expected to form SII hydrates based on the ratio comparison involving the 5^{12} cavity. However, methane ultimately forms structure I hydrates because for small, simple hydrate formers, the transition from structure II to structure I is brought about by the additional stability[4] gained by the guest molecule in the $5^{12}6^2$ cavity. This can be rationalized by examining the guest:cavity size ratio of methane to the cavities $5^{12}6^2$ (diameter ratio = 0.757) and $5^{12}6^4$ (diameter ratio = 0.675), respectively. Carbon dioxide is also expected to form SI hydrates based on similar comparisons.

Cavity occupation in structure I and structure II hydrate is determined to a large degree by the size, and to a lesser degree, by the chemical nature and shape of the guest molecules. Simple hydrates will generally have more water molecules than the ideal hydrate composition since not all of the cavities are occupied. Researchers have found that occupancy of the smaller cages of simple hydrates is incomplete for molecules with diameters less than 5.0 Å, whereas the larger cages of both structures seem to be almost completely occupied.[16] The ratios of gas molecules to water molecules usually range from Gas:$5\frac{3}{4}H_2O$ to Gas:$19H_2O$, with typical occupancies of the smaller cavities around 70% to 90%.[17] This variation leads to the designation of clathrate hydrates as "non-stoichiometric hydrates". The most non-stoichiometric guest molecules appear to be those with molecular diameters approaching the diameter of the free cavity.[18]

Guest Molecules of Structure H

Unlike structures I and II, structure H is considered a double hydrate because it requires the presence of two types of guest species to be stable. Small gas molecules, such as methane or hydrogen sulfide, are needed to occupy and stabilize the smaller cavities while larger molecules, like cyclohexane and methylcyclohexane, fill the larger cavities. Ripmeester and Ratcliffe have identified 24 SH hydrate formers.[19] These molecules include substituted methylbutanes and cycloalkanes, many of which constitute a small fraction of crude oil. These species are in the size range of 7.5 to 8.6 Å, and can be accommodated by the $5^{12}6^{8}$ cavity of structure H. Recent data reported by Lederhos et al.[15] for the methane/adamantane/water system showed that SH hydrate crystals form at pressures lower than those required to form methane simple hydrates at the same temperature. Other similar work[20] suggests that these lower formation pressures indicate that structure H hydrates involving liquid hydrocarbons are extremely stable.

Hydrate Prevention

Understanding the thermodynamics of hydrate formation is of key importance for avoiding problems with unwanted hydrate formation. Clathrate hydrate formation can be prevented by several methods based on equilibrium thermodynamic considerations. These methods include (a) removing free water, as well as reducing the water content of the hydrocarbon phase; (b) maintaining system temperature at a point above the hydrate formation temperature; (c) maintaining system pressure at a point below the hydrate formation pressure; and (d) injecting inhibitors such as methanol or ethylene glycol so that lower temperatures or higher pressures are required to form hydrates. Hydrate formation is inhibited with methanol or ethylene glycol injections because the resulting water-solute interactions interfere with the hydrophobic hydration necessary for hydrate formation.[21-22] These four methods either alter the phase diagram (water removal and injections of chemical inhibitors) or the operating conditions (heating and depressurization) to avoid production of solid hydrates. Thus, appropriate knowledge of thermodynamic[3,23-25] conditions of hydrate formation can enable the gas pipelines to be operated outside the hydrate forming conditions. The kinetics of hydrate chemistry is also important, as flow is not impeded even at conditions inside the thermodynamic phase envelope if the system remains metastable.

Hydrate Formation and Decomposition

The hydrate formation process is proposed to be closely related to more conventional crystallization processes and has been extensively studied. As in crystallization, the hydrate formation process[11,26-30] may be divided into the nucleation and growth phases. In the nucleation phase, hydrate nuclei or precursors are generated in a supersaturated aqueous solution. This phase ends with the appearance of critical sized, stable hydrate nuclei. In the growth phase, the hydrate nuclei grow as solid hydrate crystals.

An overview of the hydrate formation hypothesis is diagrammed in Figure 2-5. The diagram describes the progress of molecular species from water [A] through labile clusters [B] to metastable agglomerates [C] to stable nuclei [D], where the nucleation period ends and the growth process starts. Initially, there are no gas molecules dissolved in the water [A] even though the temperature and pressure are in the appropriate hydrate forming region. As gas molecules dissolve into the water, labile clusters [B] form immediately. These labile clusters agglomerate by sharing faces to form structures that are long-lived but unstable. These agglomerates [C] are in quasi equilibrium with each other and the labile clusters until they exceed the critical radius. When these agglomerates reach a critical size, they become nuclei [D] for immediate hydrate growth. The time needed for these stable nuclei to form is referred to as the induction time.

When a system is heated, the process described above is driven back to the left and the stable hydrate crystals are dissociated. When the hydrate dissociation temperature is exceeded, bulk hydrate disappears but microscopic species can remain in the water at temperatures up to about 20 K beyond the dissociation temperature.[31-32] These species range in size from a single labile cluster [B] to agglomerates [C]. The presence of these micro-structures in solution can promote nucleation and thus hydrate growth on further cooling.

Various experiments[7,33-34] have been done to study the effects of the thermal history of water on the induction

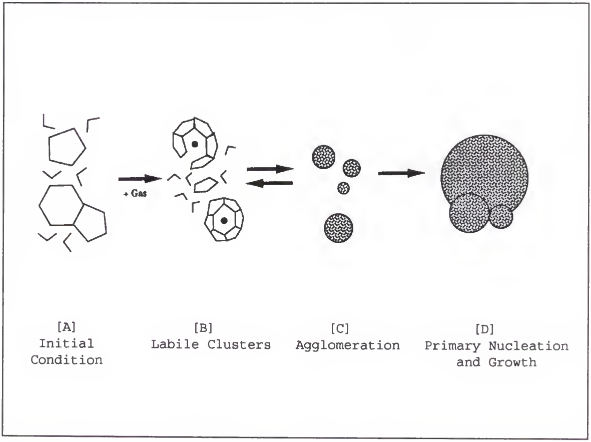

Figure 2-5. Overview of a proposed hydrate formation process.[11]

time. A shorter induction time was required for hydrate growth when water obtained from thawed ice was used than when hot water was used. Moreover, an even shorter induction time was needed for a system using water from recently dissociated hydrates than one using water from thawed ice. This effect is shown in Figure 2-6, using a pressure-temperature diagram, where successive cyclical runs were carried out on a system. The initial cooling run to form hydrates is shown with curve S_1. The container was then heated and hydrates dissociated along the vapor-liquid water-hydrate($V-L_w-H$) line until the point where the last hydrate crystal disappeared (labeled H in the figure). The sample container was then cooled to form hydrates, following curve S_2. Successive cooling curves S_2 and S_3 showed a shorter induction time because of residual hydrate micro-structures present in the water.

The results illustrated in Figure 2-6 indicate that the hydrate decomposition process is not plagued with the hysteresis often encountered in hydrate formation. In all of the heating runs described above, the hydrate sample dissociated along the $V-L_w-H$ curve, ending with complete hydrate decomposition at point H.

The hydrate decomposition process has not been as extensively studied as hydrate formation. Hydrate decomposition has been proposed to be a sequence of the host lattice destruction, followed by gas desorption as

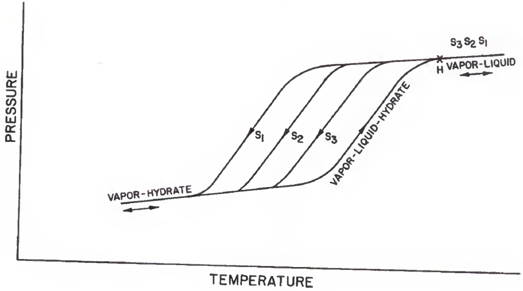

Figure 2-6. Diagram showing the water thermal history effects on the induction delay during hydrate formation.[35]

the guest molecules are freed from the cages. The onset of hydrate decomposition is usually noted by a slight increase in system pressure, which precedes a dramatic pressure jump upon complete decomposition.

CHAPTER 3
EXPERIMENTAL

A high-pressure visual cell was designed and fabricated for the study of the phase equilibria behavior of clathrate hydrates. Initially, a set of experiments was performed using methane and de-ionized water to study the growth of methane hydrates and their decomposition. Preliminary results confirmed the validity of the apparatus design as a tool for observing hydrate growth and dissociation. In subsequent experiments, observations were made while warming the cell to take advantage of the absence of water memory effects during hydrates decomposition. In this manner, the temperature and pressure at which hydrates of a particular system dissociated were easily determined.

Gases & Chemicals

The methane gas (Scott Specialty Gases) used in all the experiments had a purity greater than 99.99 mole percent. The carbon dioxide (Scott Specialty Gases) had a purity greater than 99.999 mole percent. Both gases were used as received without further treatment. Doubly-distilled water from a MilliPore Milli-Q UV Plus UltraPure Water System was used. Methylcyclohexane (practical grade) from J.T. Baker

Chemical Company, 2-methylbutane (certified A.C.S. grade) from Fisher Scientific and 2,4-pentanedione (grade not specified by manufacturer) from Eastman Kodak Company were used in the experiments. No further analysis or treatment was done on these chemicals.

Hydrate Cell

The heart of the experiment was the hydrate cell. This brass hydrate visual cell was designed and fabricated to operate safely at pressures up to 10.3 MPa (1,500 psia). Brass was used as the construction material because of its high thermal conductivity, so the cell and its contents could reach thermal equilibrium quickly during heating and cooling runs. Careful consideration was required in the design of the cell, as its full assembly would have to be seated on a microscope stage with sufficient room for adjustment.

The cell was composed of three major plates, as shown in Figure 3-1. Each brass plate was machined to a diameter of 2.250 inch. The top and bottom plates were machined to a thickness of 0.375 inch, whereas the middle plate had a thickness of 0.410 inch. A six-hole, 1.750 inch diameter bolt circle (DBC) was drilled in all three plates. For the top plate, the six holes were drilled through to clear 0.189 inch and counterbored to a diameter of 5/16 inch by 0.188 inch deep for #10 Allen cap screws. The bolt circle holes

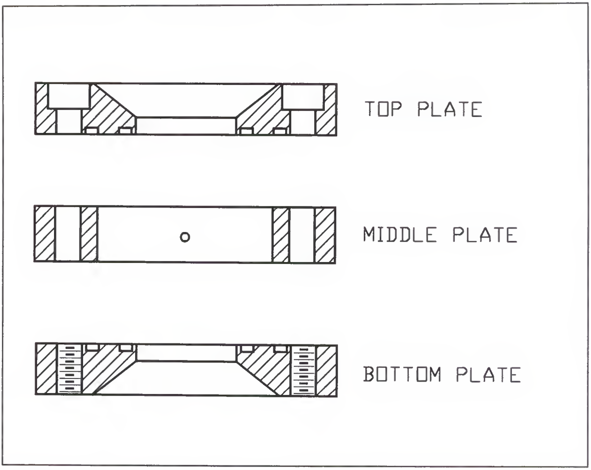

Figure 3-1. Side view of the three plates of the hydrate visual cell.

of the middle plate were drilled through to clear 0.189 inch. The six-hole bolt circle of the bottom plate was drilled and tapped for 10-32 screws. For viewing purposes under the microscope, the top and bottom plates were bored to provide a 0.750 inch diameter opening.

The top and bottom plates served to resist the internal pressure and to accommodate O-rings used to seal against leakage. Two grooves, 0.050 inch deep, were cut on each plate to accommodate 2-020 and 2-028 O-rings as shown in Figure 3-2. The middle plate comprised the heart of the apparatus. A 1.313 inch opening was cut in the center of this plate to hold a teflon ring. Grooves were cut in the teflon ring to support two sapphire windows. Figure 3-3 shows the drawings of the two teflon support rings as well as the sapphire window used in these experiments. Teflon ring I was utilized in the methane/water study, where the copper-constantan thermocouple was used as the temperature-sensing device. Teflon ring II, composed of two identical halves, was used with all other experiments where a miniature RTD was used as the temperature-sensing device. The teflon ring was then sandwiched in between the two sapphire windows, as shown in Figure 3-4, to create a compartment to contain hydrate-forming components. The total internal volume of the sample compartment was approximately 1.0 ml.

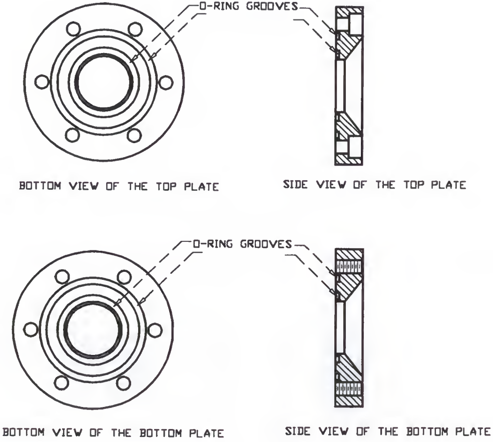
O-RING GROOVES
BOTTOM VIEW OF THE TOP PLATE
SIDE VIEW OF THE TOP PLATE
O-RING GROOVES
BOTTOM VIEW OF THE BOTTOM PLATE
SIDE VIEW OF THE BOTTOM PLATE

Figure 3-2. Views of the top and bottom plates of the hydrate visual cell.

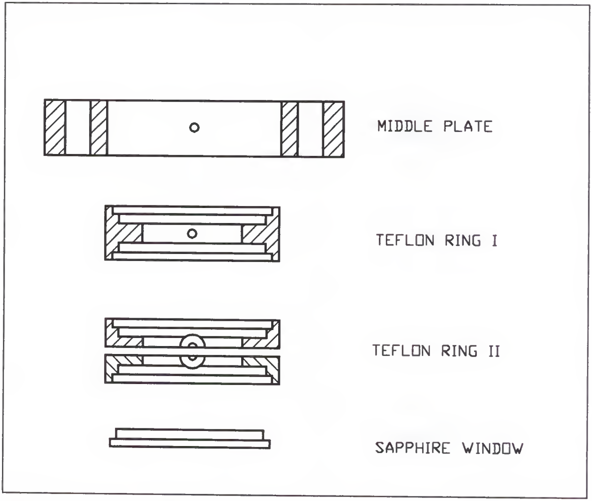

Figure 3-3. Side view of the middle plate along with the teflon ring used to hold the two sapphire windows.

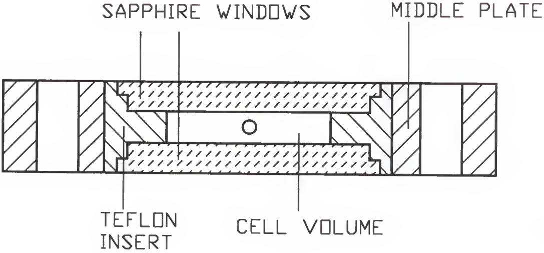

Figure 3-4. Complete assembly of the middle plate showing the teflon insert, sapphire windows and the cell volume.

A 1/16 inch hole was drilled through the side of the middle brass plate, as well as the teflon ring, for gas inlet to fill and purge the cell. Stainless steel tubing (304SS) with 1/16 inch OD was soldered to this opening. In an initial version, a similar-sized hole was drilled 180° from the gas inlet opening, to allow for temperature sensing via a copper-constantan thermocouple (Omega Engineering). This opening was pressure-sealed with an Apiezon W wax. Figure 3-5 shows the arrangement of the openings. The sensing junction of the thermocouple was placed directly in the sample. This arrangement was used for all trials involving the methane/water system. Figure 3-6 shows the complete hydrate visual cell assembly.

For trials where liquid hydrocarbons were involved, the apparatus was modified to include a hollow brass finger, as shown in Figure 3-7, which was soldered onto the middle brass plate. The wall thickness of the brass finger was 0.018 inch. This finger provided a low resistance path for heat flow to and from the enclosed temperature sensor as well as a heat exchange source with hydrates in its vicinity. A 0.120 inch diameter miniature RTD (Omega Engineering) was inserted in the brass finger to measure temperature in the cell. The brass finger arrangement was used in place of the thermocouple to avoid the problem with liquid hydrocarbons dissolving the wax used to seal the

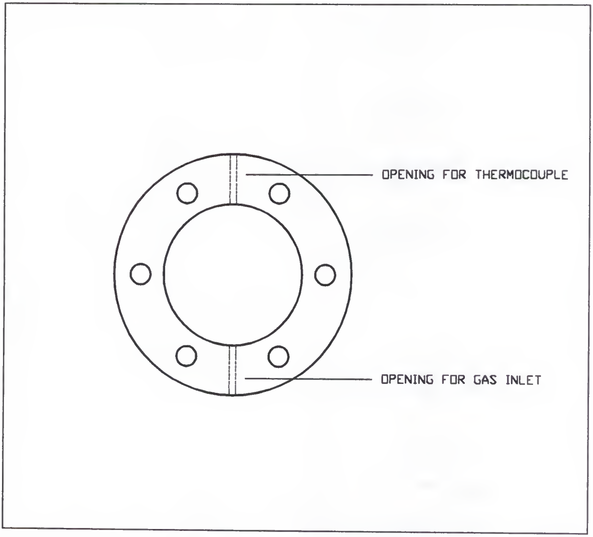

Figure 3-5. Top view of the middle brass plate, showing openings for a temperature sensing device and gas inlet.

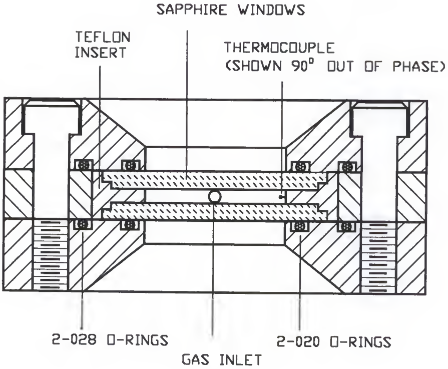

Figure 3-6. Side view of the complete assembly of the high-pressure visual hydrate cell, utilizing a thermocouple as the temperature sensing device.

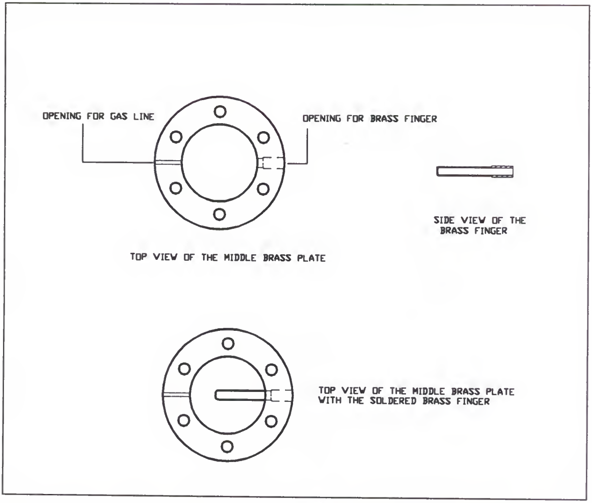
OPENING FOR GAS LINE
OPENING FOR BRASS FINGER
SIDE VIEW OF THE BRASS FINGER
TOP VIEW OF THE MIDDLE BRASS PLATE
TOP VIEW OF THE MIDDLE BRASS PLATE WITH THE SOLDERED BRASS FINGER

Figure 3-7. Top view of the brass middle plate, showing the brass finger designed to hold an RTD for temperature sensing.

temperature-sensing opening. The complete hydrate cell assembly utilizing the brass finger is shown in Figure 3-8.

A 0.100 inch diameter steel ball was placed in the sample compartment of the hydrate cell to enable mixing via an external magnet. Mixing ensured the homogeneity of the sample and was useful for promoting rapid hydrate growth. Temperature control was achieved by placing the hydrate cell in a square, foam-insulated brass block. This block is shown in Figure 3-9. The square brass block was machined to have the dimensions of 3.000 inch by 3.000 inch with a thickness of 1.500 inch. A 2.260 inch hole was cut in the middle of the block to contain the hydrate cell. The block was designed to be cooled by the circulation of a 50/50 by volume solution of diethylene glycol-water, which was connected to a Fisher Scientific Chiller. The chiller was capable of controlling the coolant's temperature to ± 0.1 K, although the temperature of the cell was measured with a sensor placed directly in the sample compartment.

Interfacing

All components of the hydrate cell were linked to a Gateway 2000 micro-computer for data acquisition. The computer contained a 486 internal processor operating at 66 megahertz with 32 megabytes of RAM. The interfacing protocol used for the connection of the electronic hardware to the micro-computer was the standardized IEEE general

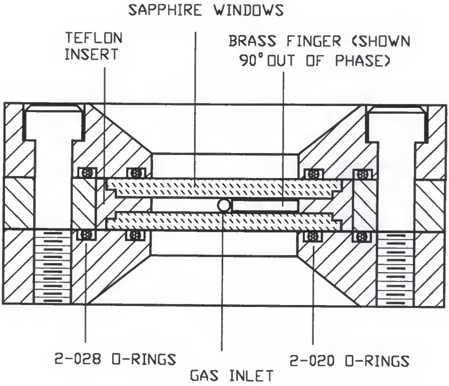

Figure 3-8. Side view of the completely assembled high-pressure visual hydrate cell, utilizing a brass finger for the insertion of an RTD as the temperature sensing device.

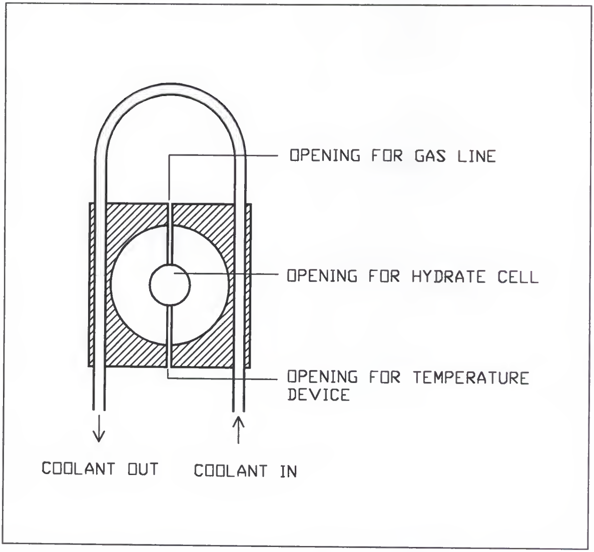

Figure 3-9. Top view of the block used for temperature control of the hydrate visual cell.

purpose bus interface (GPIB), including the 8-bit i/o card and the accompanying software. The electronic equipment used the in the experiments contained the IEEE connection interface when purchased.

Measurement Hardware

The fully assembled cell along with the cooling block was placed on the microscope stage. The microscope used in all experiments was a Nikon Optiphot2-POL. A Sony CCD/RGB Model DXC-151 Color Video Camera, mounted over the microscope, provided an enlarged viewing image of the sample. A television (TV) and a video cassette recorder (VCR) were wired to the camera for the direct recording of activity inside the hydrate cell. The schematic setup of the electronic hardware used in the experiments is shown in Figure 3-10. Each physical property measurement required a specific protocol for acquisition. The following two sections describe the measurement procedures, in addition to details of the electronic hardware, summarized in Table 3-1.

Pressure

Pressure data were acquired with a Sensotec model TJE/713-22 strain gage pressure transducer with an effective pressure range of 0-1,000 psi. This pressure transducer was used together with a Beckman Industrial 600 Series electronic readout device. The Sensotec transducer was

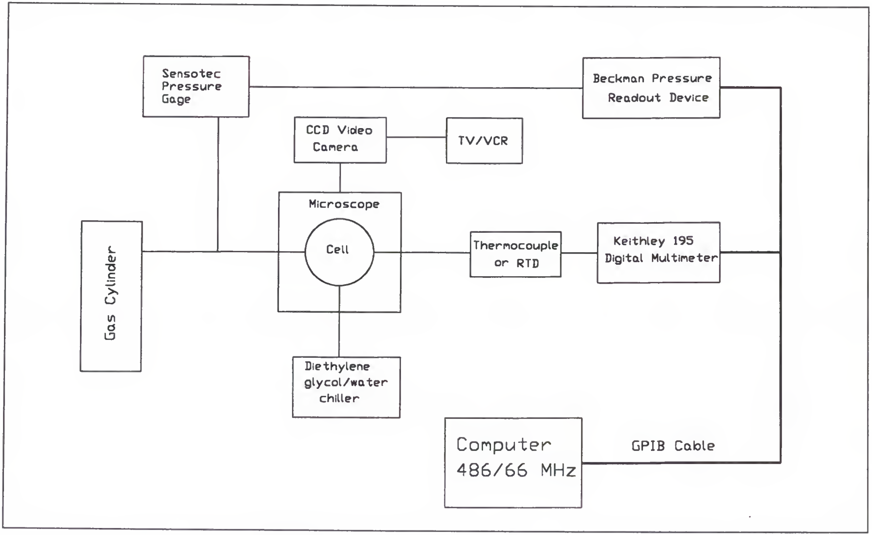

Figure 3-10. Schematic diagram of the electronic hardware setup.

Table 3-1. Summary of measurement hardware.

Item	Manufacturer	Model Number	Range of Operation	Resolution (manufacturer's stated value)	Function
Digital strain gage transducer indicator	Beckman Industrial Corp.	600 Series	-150 mV to 1 V	± 0.01% full scale	Accepts strain gage transducer input.
Strain gage pressure transducer	Sensotec	TJE 713-22	0-1,000 psia	± 0.01% full scale	Measures pressure.
Thermocouple (Copper-Constantan)	Omega Engineering Inc.	SPCP-005 SPCC-005	-270 to 400 °C	± 1.0 °C	Measures temperature in voltage.
RTD	Omega Engineering Inc.	W2102	-50 °C to 600 °C	± 0.1% Ohms.	Measures temperature in resistance.
Digital Multimeter	Keithley Instruments Inc.	K195A	20mV to 1000V; 20 Ω to 20 MΩ, 2 or 4-terminal resistance measurements.	Range dependent, see manufacturer's manual for details.	Measures voltage or resistance from temperature probes.

calibrated against a Ruska Model 2465 standardized Dead Weight Pressure Gage. The Ruska gage had a pressure range of 0.000 psia to 650.000 psia with an accuracy of ± 0.001 psia. Figure 3-11 shows the pressure calibration results.

Temperature

A type T (copper-constantan) thermocouple was initially used as the temperature sensor. Uninsulated base metal copper and constantan wires were obtained from Omega Engineering. The ends of these 0.005 inch diameter wires were heated and melted together to create the sensing and reference junctions. The reference junction was placed in an ice bath at 0 °C. The wiring diagram for the thermocouple is shown in Figure 3-12. This thermocouple was wired to a Keithley 195A digital multimeter which was set to operate in the voltage mode. Voltage values were converted to temperature, in Celsius, using the following equation,

$$T = a_0 + a_1 x + a_2 x^2 + \ldots + a_n x^n .$$

In this equation, x is voltage and the coefficients, provided by the manufacturer, are:

a_0	0.100860910	a_4	-9247486589
a_1	25727.94369	a_5	6.97688×10^{11}
a_2	-767345.8295	a_6	-2.66192×10^{13}
a_3	78025595.81	a_7	3.94078×10^{14}

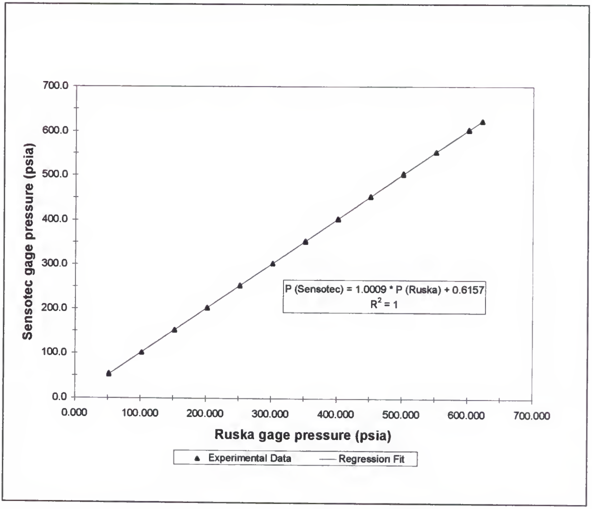

Figure 3-11. Pressure gage calibration data using methane gas at 298 K.

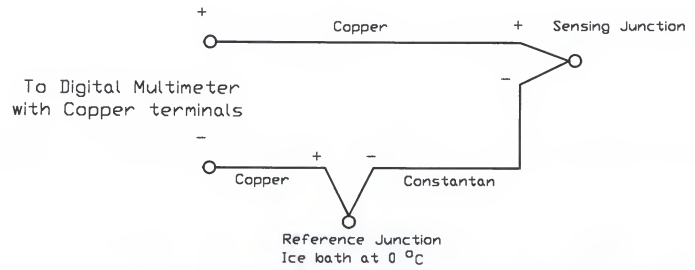

Figure 3-12. Wiring diagram for the copper-constantan thermocouple.

The manufacturer's stated uncertainty in temperature measurement using the thermocouple was ± 1.0 °C.

Additionally, a two-wire platinum resistance temperature device (RTD) was used in most of the experiments. The ceramic, cylindrically-shaped RTD was used in conjunction with the same Keithley 195A digital multimeter to read resistance data. The resistance values were converted to their corresponding temperatures, in Celsius, using the following equations and parameters,

$$A = \alpha\left(1 + \frac{\delta}{100}\right)$$

$$B = -\alpha\,\delta\,(0.0001)$$

$$T = \frac{-A + \sqrt{A^2 - 4B\left(1 - \frac{R_t}{R_o}\right)}}{2B}$$

where $\alpha = 0.00385$, $\delta = 1.502$, $R_o = 100.00\ \Omega$, and R_t is the resistance of interest.

The Beckman readout device and the Keithley multimeter were interfaced to the micro-computer via the IEEE general purpose interface bus (GPIB). Pressure and temperature data were acquired with computer programs written specifically for these experiments. These programs were written using the ANSI C standard code language and are listed in Appendix A.

CHAPTER 4
EXPERIMENTAL PROCEDURE

Initially, all components of the hydrate visual cell were completely taken apart, cleaned with soapy water and rinsed three times with doubly-distilled water. All parts were carefully dried using Kimwipes and blowing nitrogen gas. O-rings of the appropriate sizes were lubricated with silicone grease and placed in the grooves of the top and bottom brass plates. The teflon ring was placed in the middle brass plate. One sapphire window was snapped into place on the teflon ring creating the bottom half of the cell compartment. Approximately 1.0 ml of doubly distilled water was then added drop-wise (~20 drops) to the cell compartment. A steel ball was placed inside the cell compartment to enable mixing via coupling to an external movable magnet once the cell was assembled. The second sapphire window was snapped onto the top half of the teflon ring to complete the compartment. The middle brass plate was then placed in between the top and bottom brass plates. Allen cap screws (10-32) were used to seal the system.

The hydrate cell was connected to the gas supply tank using 1/16 inch stainless steel tubing. Prior to charging the cell, these lines were purged with gas (either methane or carbon dioxide, depending on the experiment) at an approximate pressure of 50 psi. This same pressure was applied continuously to the hydrate cell as it was connected to the gas supply. The cell was charged to an appropriate pressure with the gas of interest. It was then placed in the cooling block for temperature control and positioned on the microscope stage. The image seen under the microscope was captured with a CCD video camera mounted on the microscope and displayed on a monitor. A VCR was wired to the monitor and the hydrate formation and decomposition process could be recorded.

The chiller was turned on and connected to the cooling block. Diethylene glycol-water coolant began to circulate to bring the cell to the initial temperature. The temperature of the coolant was normally set to -5.0 °C, although the cell's temperature was measured directly by a sensor inside the cell, typically reaching around -2.0 °C. The cell was allowed to cool for about two hours while its contents were mixed periodically by using an external magnet to agitate the steel ball. Nitrogen gas was allowed to flow over the outside surface of the sapphire windows to prevent condensation and ice formation. The effects of condensation and ice formation on the external surface of the window are shown in Appendix B.

After an initial cooling period, the contents of the cell were observed with the naked eye, as well as microscopically, from the images captured with a video camera mounted on the microscope and displayed on the monitor. Typically, with any new water sample a long induction period was observed. Hydrate formation required around five hours. Prior to the onset of hydrate formation, the cell's contents became increasingly turbid with mixing. The turbidity appeared when the solution became translucent owing to the emergence of hydrate nuclei particles. Although the size[36] of these hydrate particles is too small for individual visual detection, their number is sufficiently large to make the solution appear turbid. The appearance of these hydrate nuclei in solution signifies the onset of hydrate formation. With further mixing, there was rapid hydrate growth and hydrates covered the entire sapphire window. Many researchers have noted that hydrate formation was normally accompanied by a dramatic drop in pressure, normally a change of at least 100 psi (700 kPa). However, in all experiments described here, the pressure drop due to hydrate formation was at most 10 psi (70 kPa). This small change in pressure was attributed to the small sample size (~1 g) used in this work.

The methane/water system was used initially to confirm the validity of the experimental set-up and technique for the determination of hydrate phase equilibria. Once hydrate formation was visually noted, the cell was allowed to equilibrate for another hour. For the determination of the equilibrium hydrate decomposition temperature at a particular pressure, the cell was then heated. The cell was heated at a rate of 1.0 K/10 minute until its temperature reached 1.0 K below the equilibrium temperature reported in the literature. At this point, the heating rate was reduced to 0.1 K/10 minute and the actual data acquisition of the experiment began. Temperature and pressure data were acquired about every two seconds. Appendix C shows the results of experiments performed to determine the effectiveness of the cooling block in controlling cell temperature.

Changes in the cell's contents were monitored with the help of the microscope. The onset of hydrate decomposition was dramatically highlighted by the first formation of microscopic bubbles in the cell. Heating was halted as soon as any bubble formation was detected. As the hydrate decomposition process continued, an increasingly larger number of bubbles formed and grew in size and eventually coalesced. The process was deemed complete when all the bubbles had "popped" and the viewing window under the microscope was free of bubbles. A slight increase in cell pressure, around 3-5 psi (20-35 kPa), was noted as a result of the hydrate decomposition process. The point at which bubble formation initially started was taken to be the equilibrium hydrate decomposition temperature and pressure.

Subsequent experiments on the same system were carried out by charging the cell with more gas to increase cell pressure each time by about 75-100 psi (500-700 kPa). Ordinarily, with any new loading of water, the cell was charged to around 400 psi (2.7 MPa). In this manner, approximately 5-7 trials could be completed using the same water loading. Another advantage in following this routine was that the time required for hydrate formation was reduced drastically, taking from as much as 6 hours for the first run to as little as 30 minutes on subsequent trials.

In the case of hydrate-forming systems for which phase equilibria data are not available in the literature, a heating rate of 0.5 K/minute was initially used to determine the approximate decomposition temperature. In the next run at the same pressure, the system was heated more slowly in order to obtain a more accurate decomposition temperature. This was accomplished by changing the heating rate to 0.1 K/minute when the cell's temperature reached within 1.0 K of the initial decomposition temperature. Thus, for the determination of each equilibrium data point for these systems, at least two trials were carried out at a given pressure.

In experiments to study gas/liquid hydrocarbon/water systems, 10 drops of the liquid hydrocarbon were added to the cell along with 10 drops of doubly-distilled water. Thus, an approximate ratio of 50/50 by volume of liquid hydrocarbon to water was used in these trials. A procedure similar to the one described in the preceding paragraphs was followed.

In all experiments, temperature and pressure data over the range of interest were recorded as a function of time while the cell was heated until hydrate decomposition was detected. The cell's contents were viewed on the monitor, and the visual information was recorded on a videotape for subsequent review.

The experimental procedure took advantage of the univariance of the system as established by the Gibbs' phase rule. The rule allows for the calculation of the number of phases that can coexist in equilibrium in a given system, or if the number of phases is given, of the number of degrees of freedom. Gibbs' phase rule is given by,

$$\Phi = C + 2 - P$$

where Φ, C and P are the degrees of freedom, number of components and the number of phases, respectively. For example, in the three-component methane + methylcyclohexane + water system, where four phases coexist at equilibrium; namely: liquid water, liquid methylcyclohexane, vapor and structure H hydrate, the phase rule requires that there be exactly one degree of freedom. Consequently setting the temperature at which the four phases coexist at equilibrium would uniquely determine all other intensive parameters, such as gas composition, hydrate composition, and pressure.

CHAPTER 5
HYDRATE DECOMPOSITION IMAGES

Visual information from each hydrate decomposition run was continuously recorded on videotape. Images of interest were then captured frame by frame, using the commercial hardware Snappy video snapshot from Play Incorporated, and saved as computer files in the graphical image format (GIF). Figures 5-1 to 5-6 show typical microscopic snapshots of the hydrate cell's contents as the cell was heated to determine its decomposition temperature and pressure. The images were of a run involving the methane/methylcyclohexane/water system; similar behavior was observed for all hydrate-forming systems examined in this research.

Figure 5-1 shows the cell's contents at a temperature and pressure before hydrate decomposition begins. At this point, there were no bubbles in the hydrate mass shown in the viewing window. The onset of the hydrate decomposition is seen in Figure 5-2, as evidenced by the formation of a small number of microscopic methane gas bubbles. Figure 5-3 shows the cell's contents at 0.1 K into the decomposition process. More gas bubbles were seen in the cell. This behavior suggests that as the decomposition temperature was reached, some water cages started to break apart. The collapse of these cages released methane molecules, in the form of microscopic bubbles, into the gas phase. A pressure increase of about 2 psi (14 kPa) was noted at this point. At this time, heating of the cell was halted. As the cell's temperature was held constant, decomposition continued as evidenced by the formation of an increasingly larger number of bubbles. After a 15-minute waiting period, the bulk hydrate mass had not completely dissociated. Heating was resumed at a rate of 0.1 K/10 minute.

At a temperature over 1 K into the decomposition process, as shown in Figure 5-4, bubbles filled the entire viewing window of the microscope. These observations suggested that, for a system at a given pressure, the clathrate hydrates did not completely dissociate at one specified temperature. Rather, hydrate decomposition began at a particular temperature and continued as the cell was slowly heated. Because the experiment is performed under isochoric conditions on a fixed sample, it measures points along a short length of the PT phase equilibrium line. The gas released by hydrate decomposition increases the system pressure, and the equilibrium temperature increases in step.

Figure 5-5 shows the cell's contents at around 293 K. At this point, many large bubbles were observed to remain in the cell. However, all of the bulk hydrate mass had dissociated. Visual observations indicated that the solution was still very turbid. Solution turbidity suggested the lingering presence of hydrate nuclei particles in the cell. If the cell was cooled below the decomposition temperature at this time, these microstructures would immediately promote hydrate growth. Several experiments were later carried out which confirmed this expected behavior. In Figure 5-6, the cell's temperature had reached 300.5 K. Most of the bubbles have disappeared at this point. A system pressure increase of about 8 psi (55 kPa) was recorded for this complete run.

In the determination of phase equilibria for any hydrate-forming system, the temperature and pressure when microscopic gas bubbles began to form were recorded as the hydrate decomposition point. This formation of these microscopic bubbles undoubtedly signifies arrival at the hydrate phase envelope. Bubble formation at this level has not been previously reported by other researchers. In the hydrate-forming system described previously, the temperature and pressure conditions remarked in Figure 5-2, specifically 286.8 K and 6.342 MPa (919.9 psi), would be recorded as the hydrate decomposition point.

Several experiments were carried out to study whether bubble formation was unique to hydrate-forming systems. In these trials, the cell was filled with only doubly-distilled water and cooled to 271 K overnight to form ice. None of the liquid hydrocarbon nor any of the gas was added to the cell. Upon heating, visual observations using the microscope indicated no bubble formation. The solid mass completely melted as the temperature reached 273.7 K.

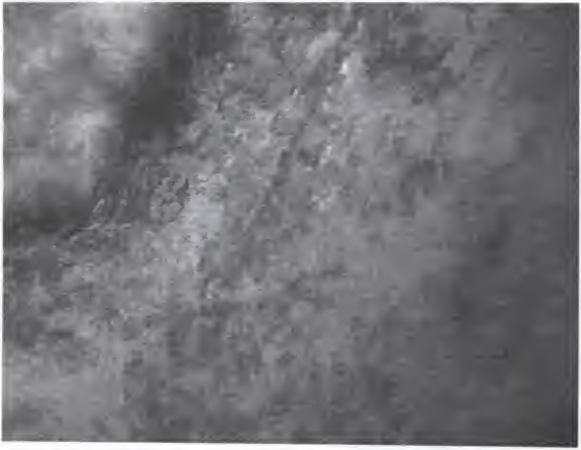

Figure 5-1. Image of the cell's contents moments before reaching the hydrate decomposition temperature.

Temperature = 286.1 K Pressure = 6.331 MPa (918.3 psi)

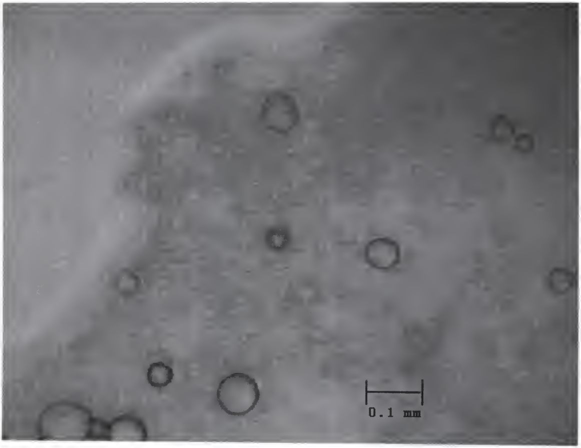

Figure 5-2. Onset of hydrate decomposition as noted by a small number of methane gas bubbles coming up to the surface.

Temperature = 286.8 K Pressure = 6.342 MPa (919.9 psi)

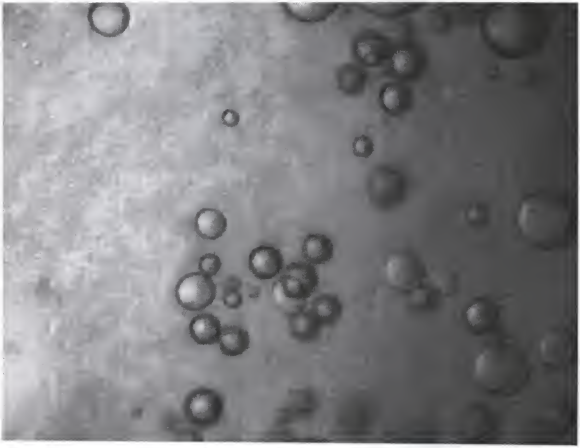

Figure 5-3. Moments after the decomposition process started, showing more methane gas bubbles forming at this point.

Temperature = 286.9 K Pressure = 6.345 MPa (920.3 psi)

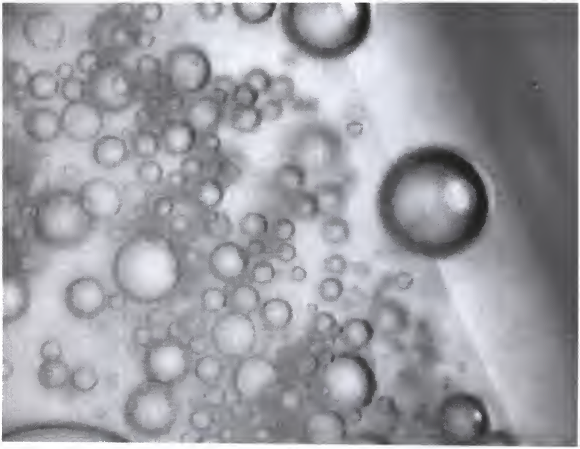

Figure 5-4. Image of the cell's contents at nearly one degree after the start of the hydrate decomposition process. Bubbles filled the entire viewing window of the microscope.

Temperature = 287.5 K Pressure = 6.358 MPa (922.1 psi)

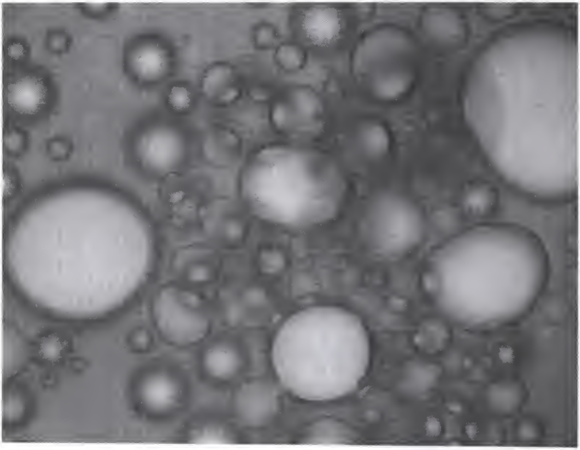

Figure 5-5. Many large bubbles could be seen lingering in the cell at a temperature well past the decomposition temperature.

Temperature = 293.0 K Pressure = 6.370 MPa (923.9 psi)

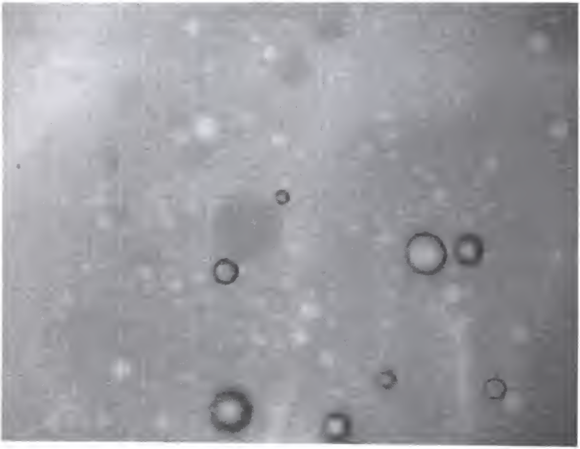

Figure 5-6. Image of the cell's contents at nearly 15 degrees past the decomposition temperature. Most of the bubbles have "popped".

Temperature = 300.7 K   Pressure = 6.387 MPa (926.3 psi)

CHAPTER 6
RESULTS

Structure I Hydrates

Phase equilibria measurements on the methane system provided initial confirmation of the new technique for detection of the onset of hydrate decomposition. Water is an essential component for the formation of clathrate hydrates. Thus, the methane system is understood to be the methane/water system, and this designation will be used throughout this chapter. The methane system was selected for this study because it is the one that has been most extensively studied by other researchers[37-42] and for which there exists the most extensive pool of data for comparison.

Methane

Data were collected over a pressure and temperature range of 2.8 MPa to 7.0 MPa and 273 K to 283 K, respectively. Temperature readings for experiments on this system were obtained using the copper-constantan thermocouple. In all subsequent systems studied, the platinum RTD was used as the temperature-sensing device. Phase equilibria data of water-rich liquid, hydrate and vapor for methane are tabulated in Table 6-1. Figure 6-1 shows these data graphically on a pressure versus temperature plot. A comparison of the experimental phase equilibria to the data reported in the literature shows the potential of this apparatus in obtaining comparable results. Methane hydrate data reported by other researchers were compared to this work and shown in Figure 6-2.

An exponential function was used to fit the methane experimental data of this work. The function had the form,

$$P_{calc} = Be^{A \bullet T} \tag{6-1}$$

In this equation, P_{calc} is the pressure in kPa, T is temperature in Kelvin. The values for the constants are, $A = 0.1009\ K^{-1}$ and $B = 2.79\ x10^{-9}$ kPa. A plot of ln P_{calc} versus temperature of the experimental data yielded a straight line with a chi-squared value of 0.9991. Also listed in Table 6-1 are the relative percent deviation in experimental pressures from values calculated using this empirical fit.

Carbon Dioxide

The next structure I hydrate-forming system studied involved carbon dioxide. This system has also been extensively studied by other researchers.[37-38,43-45] Phase equilibria data were collected over a pressure range of 1.4 MPa to 6.0 MPa and temperatures from 273 K to 283 K. The data obtained from measurements on this system are listed in

Table 6-1. Experimental phase equilibria data for the methane system along with relative percentage deviation in pressure from an empirical fit.

Temperature (K)	Pressure (MPa)	% Deviation
274.0	2.839	-0.5
274.2	2.892	-0.6
274.3	2.943	0.1
274.4	3.011	1.4
274.9	3.138	0.5
275.4	3.241	-1.3
275.5	3.352	1.0
276.0	3.508	0.5
276.1	3.532	0.2
276.4	3.564	-1.9
276.9	3.836	0.4
277.0	3.871	0.3
277.5	4.002	-1.4
277.8	4.178	-0.2
277.8	4.136	-1.2
278.4	4.468	0.5
279.1	4.758	-0.3
279.3	4.924	1.1
279.9	5.256	1.6
280.1	5.339	1.2
280.4	5.510	1.3
280.9	5.743	0.4
281.2	5.883	-0.3
281.9	6.328	0.0
282.0	6.406	0.2
282.1	6.444	-0.2
282.2	6.520	-0.1
282.4	6.633	-0.4
282.5	6.671	-0.8
282.7	6.811	-0.7

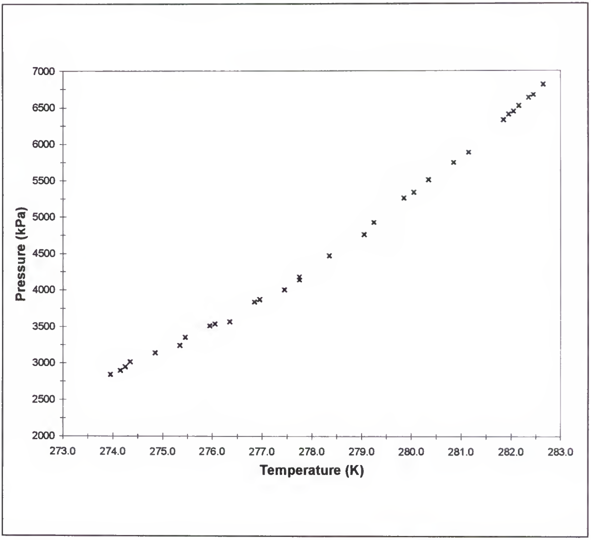

Figure 6-1. Plot of the experimental phase equilibria data for the methane system.

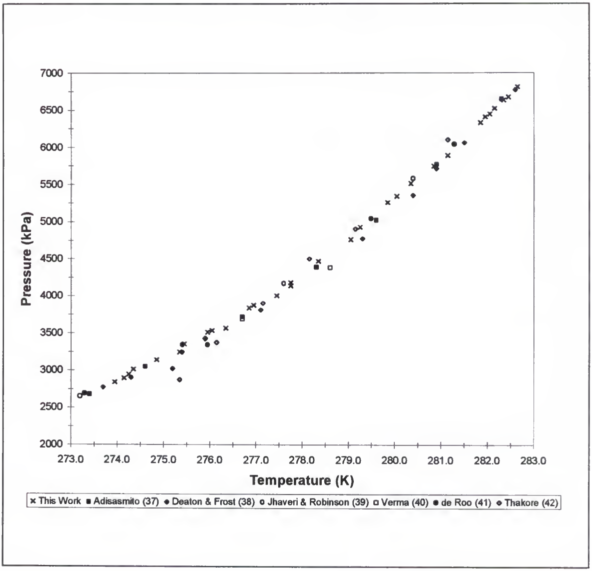

Figure 6-2. Comparison plot of phase equilibria data for the methane system.

Table 6-2 and shown graphically as a pressure versus temperature plot in Figure 6-3. As noted from the plot, the hydrate equilibrium system pressure rises rapidly at temperatures above 282 K. This is due to the occurrence of a second phase transition, namely the condensation of gaseous carbon dioxide to liquid at pressures above 4.37 MPa.[37] Figure 6-4 shows a comparison plot of the results from this work with those of other researchers.

These data were also fitted with the equation of the form,

$$P_{calc} = Be^{A \bullet T}.$$

Data corresponding to pressures below and above 4.37 MPa were fitted separately. The constants for the fit of data below 4.37 MPa are, $A = 0.1291\ K^{-1}$ and $B = 5.91 \times 10^{-13}$ kPa. A plot of ln P_{calc} versus temperature of the experimental data yielded a straight line with a chi-squared value of 0.997. The fit of data above 4.37 MPa yielded values of $A = 0.7049\ K^{-1}$ and $B = 1.13 \times 10^{-83}$ kPa. An ln P_{calc} versus temperature plot of the experimental data yielded a straight line with a chi-squared value of 0.818. Also listed in Table 6-2 are the relative percent deviation in experimental pressures from values calculated using this exponential empirical fit.

The experimental results from these two hydrate-forming systems have proven the cell's functionality in determining

Table 6-2. Experimental phase equilibria data for the carbon dioxide system along with relative percentage deviation in pressure from an empirical fit.

Temperature (K)	Pressure (MPa)	% Deviation
274.31	1.424	0.2
274.32	1.418	-0.4
275.56	1.660	-0.7
275.96	1.760	0.0
277.60	2.149	-1.2
277.85	2.289	1.9
278.65	2.528	1.5
279.45	2.875	4.1
279.95	2.921	-0.8
280.36	3.023	-2.6
280.75	3.320	1.7
281.15	3.384	-1.6
281.17	3.387	-1.8
281.60	3.703	1.6
282.76	4.435	5.7
282.77	4.348	2.9
282.82	4.431	1.3
282.84	4.482	1.0
282.93	4.525	-4.3
282.95	4.575	-4.6
283.02	4.729	-6.1
283.05	4.862	-5.5
283.10	4.906	-7.9
283.11	5.533	3.1
283.15	5.944	7.7
283.17	5.890	5.2
283.21	5.979	3.8

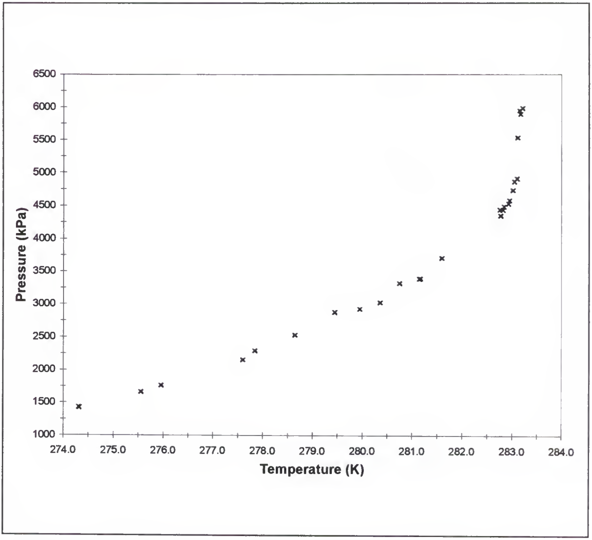

Figure 6-3. Plot of the experimental phase equilibria data for the carbon dioxide system.

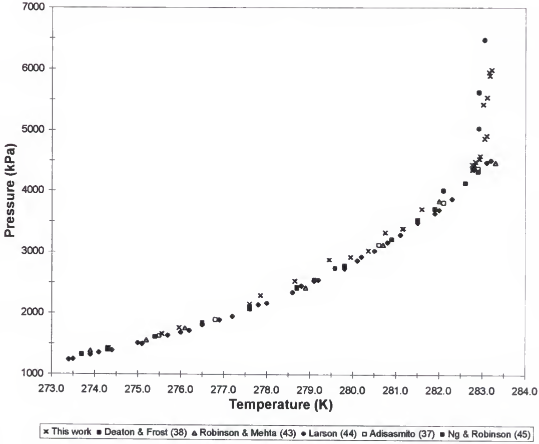

Figure 6-4. Comparison plot of phase equilibria data for the carbon dioxide system.

the onset of hydrate decomposition, generally, in good agreement with data reported in the literature.

Structure H Hydrates of Methane

The hydrate-forming systems studied thus far are termed single hydrate systems, meaning that only one guest species is required for formation and stabilization. Molecules larger than n-butane were considered to be non-hydrate formers until the discovery of structure H hydrates in 1987.

Structure H hydrates are unique in that they require both a help gas such as methane, and a large molecule, such as n-hexane, methylcyclohexane or adamantane, which constitute a small fraction of petroleum and are typically present in crude oil reservoirs. The focus of this research was then shifted to studying structure H hydrates to illustrate the utility of the apparatus in determining phase equilibria of any system of interest.

Methane/Methylcyclohexane

These experiments were carried out using methane and the liquid hydrocarbon, methylcyclohexane. Phase equilibria data for this system were collected over a pressure range of 2.0 MPa to 7.0 MPa and 275 K to 288 K, respectively. Some peculiar behavior was observed upon hydrate decomposition. In particular, there were two regions where bubble formation occurred. This behavior will be explained shortly in the discussion section. The data obtained from measurements on this system are listed in Table 6-3. The first two columns list data corresponding to the first period of hydrate decomposition. The next two columns represent data for the second bubble formation period. These experimental data are shown in Figure 6-5 in the form of two equilibrium curves.

Methane/2-Methylbutane System

The next structure H hydrate-forming system studied involved methane and 2-methylbutane, another liquid hydrocarbon. Phase equilibria data for this system were collected over a pressure range of 2.0 MPa to 7.0 MPa and 273 K to 284 K, respectively. The data obtained from measurements on this system are tabulated in Table 6-4. Similar observations to those noted in the methane/methylcyclohexane study, namely the two bubble formation regions, were seen in all decomposition runs. These data are shown graphically on a pressure versus temperature plot in Figure 6-6.

Discussion

For the purpose of discussion, observations for the experimental run involving the methane/methylcyclohexane system with a pressure of 6.136 MPa will be described. Bubble formation, as before, was indicative of the onset of hydrate decomposition. Visual observations of the cell

Table 6-3. Experimental phase equilibria data for the methane/methylcyclohexane system.

Temperature (K)	Pressure (MPa)	Temperature (K)	Pressure (MPa)
276.03	3.436	277.08	2.199
276.40	3.556	277.60	2.234
278.17	4.211	279.27	2.741
278.20	4.161	279.60	2.831
278.25	4.160	280.01	2.939
278.86	4.657	280.25	3.086
279.03	4.675	280.45	3.169
279.20	4.646	281.60	3.396
280.04	5.204	281.78	3.454
281.45	5.717	282.18	3.805
282.23	6.329	282.49	3.922
282.35	6.174	282.59	3.859
282.42	6.327	282.89	4.177
282.65	6.536	283.00	4.182
283.03	6.891	283.77	4.664
283.05	6.909	283.99	4.704
		284.60	5.274
		285.31	5.719
		285.78	5.965
		286.11	6.183
		286.30	6.346
		286.47	6.385
		286.63	6.409
		286.90	6.560
		287.03	6.919
		287.10	6.895
		287.25	6.933

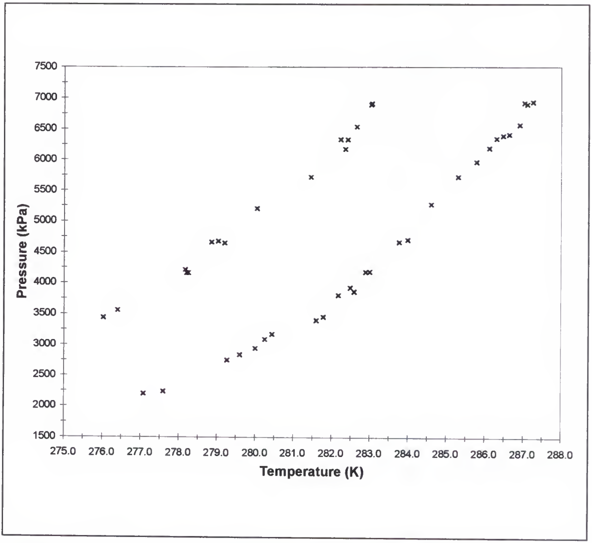

Figure 6-5. Plot of the experimental phase equilibria data for the methane/methylcyclohexane system.

Table 6-4. Experimental phase equilibria data for the methane/2-methylbutane system.

Temperature (K)	Pressure (MPa)	Temperature (K)	Pressure (MPa)
273.99	2.843	274.82	2.534
275.40	3.317	275.95	2.889
277.06	3.950	276.94	3.367
278.71	4.604	277.67	3.615
279.46	5.041	278.54	3.996
280.69	5.692	279.64	4.316
281.80	6.316	279.90	4.498
282.68	6.764	280.31	4.756
283.16	7.044	280.50	4.838
		281.33	5.357
		281.52	5.452
		282.50	6.079
		283.46	6.591
		283.99	6.846

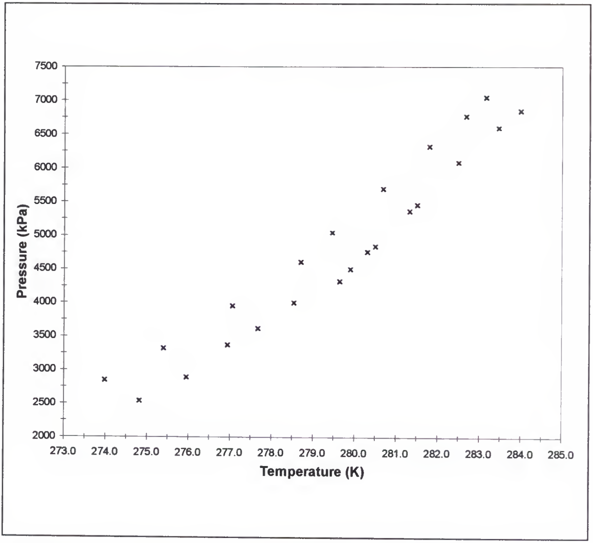

Figure 6-6. Plot of the experimental phase equilibria data for the methane/2-methylbutane system.

during warming indicated bubble formation around 282.3 K. The system pressure at this point was 6.136 MPa. Bubble formation continued, accompanied by a 21 kPa (3 psi) increase in pressure, as the cell was slowly heated. As the cell temperature rose above 283.7 K, most of the bubbles have disappeared. However, some bulk hydrate mass was still present in the cell. At this time, there occurred a total drop in system pressure of nearly 100 kPa (15 psi). This was followed by a large amount of hydrate growth, as solid hydrates formed and filled the entire cell. When the cell was examined under the microscope at this point, the viewing window was completely dark because none of the light could go through the sample. As heating of the cell continued, bubble formation was again noted at around 286.2 K. In all trials involving the methane/methylcyclohexane system, the two regions of bubble formation were approximately 3.5 K apart. For the runs involving the methane/2-methylbutane system, the two bubble formation regions were approximately 1.5 K apart.

Figure 6-7 shows a typical plot of the behavior of the system pressure during a hydrate decomposition run. The plot shows a large pressure drop at around 40 minutes, soon after the system had gone through its first hydrate decomposition/bubble formation period. This was followed by a period of hydrate growth. System pressure then slowly increased as the system was heated to its second decomposition temperature.

Figure 6-8 shows the comparison between the phase equilibria results on the methane/methylcyclohexane system with recent literature data.[10,37,51] Figure 6-9 shows the comparison plot of data of the methane/2-methylbutane system with those of other researchers.[10,37,51] In both plots, the top equilibrium curve corresponds to the methane hydrate equilibrium curve, whereas the bottom one corresponds to the hydrate of structure H equilibrium curve.

These results suggest that, upon cooling of the cell, methane structure I hydrates formed first even though the three-component structure H solid is thermodynamically favored. As the cell was heated to decompose the hydrates, the first bubble formation period appeared to be due to the decomposition of the methane hydrates (structure I). After some further heating, the formation of structure H began as indicated by the large pressure drop. The pressure drop occurred due to encapsulation of the gas molecules in the hydrate phase. The growth of the structure H hydrate appears to be promoted by the microstructures resulting from decomposition of the structure I methane hydrate. More heating eventually led to the decomposition of the structure H hydrates.

The data used for the comparison of the methane hydrate equilibrium curve are the most recent results on the methane system as reported by Adisasmito.[10] Mehta & Sloan[37] and Thomas & Behar[51] recently reported structure H equilibrium data for both of these systems and these are included in the comparison in both Figure 6-8 and Figure 6-9. Their reports, however, did not provide any coexisting equilibrium data corresponding to the decomposition of methane hydrate despite observations of similar trends regarding the transition from structure I to structure H hydrate. Naturally, investigation of this solid-to-solid structural transition are needed to understand the mechanisms of SH formation. Some preliminary results from a study of this effect in a xenon/neohexane system, using ^{129}Xe NMR analysis, have been reported.[53]

Figure 6-10 shows a comparison plot of structure H and structure I hydrates involving methane. The structure H equilibrium lines lie below the structure I line for both systems. At a given temperature, the pressures required for structure I hydrate formation is much greater than those needed to form structure H. These low formation pressures indicate that structure H hydrates involving these liquid hydrocarbon systems are extremely stable.

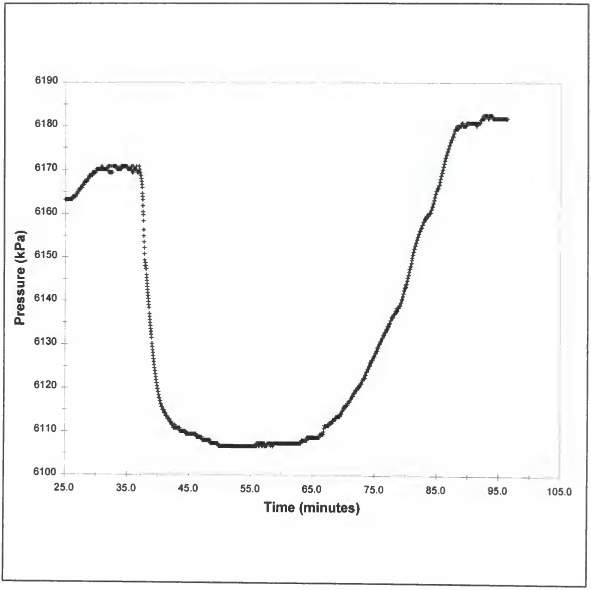

Figure 6-7. Plot of the typical behavior of system pressure during a decomposition run involving the methane/methylcyclohexane system, showing the transition from structure I to structure H.

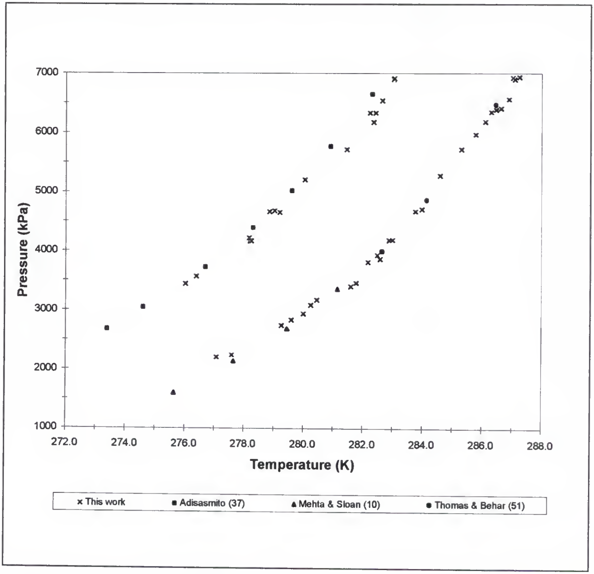

Figure 6-8. Comparison plot of phase equilibria data for the methane/methylcyclohexane system.

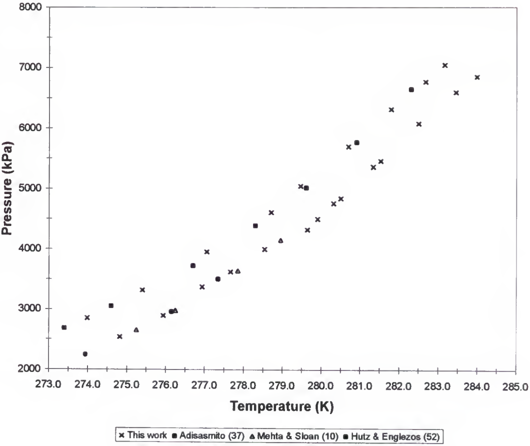

Figure 6-9. Comparison plot of phase equilibria data for the methane/2-methylbutane system.

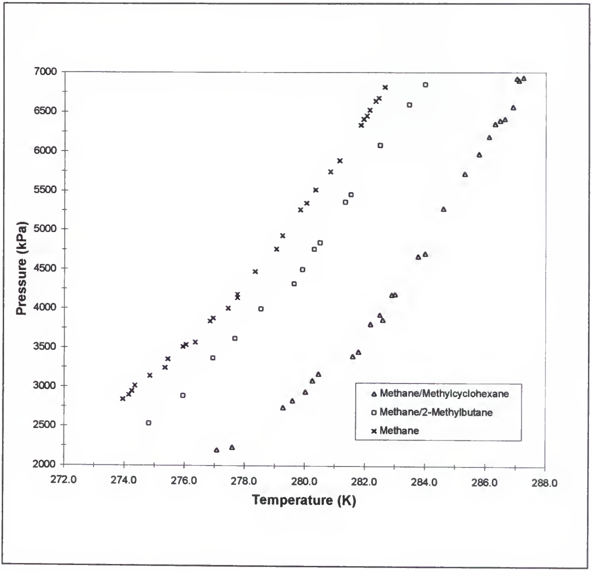

Figure 6-10. Comparison plot of the experimental data involving methane structure H hydrates with those of structure I methane hydrates.

Structure H Hydrates of Carbon Dioxide

In the following two studies, carbon dioxide replaced methane as the help gas. Occupation of hydrate cavities is determined to a large degree by size, and to a lesser degree, by the chemical nature or shape, of the guest molecule. Thus, the intention of this gas exchange was to determine whether the molecular dimensions of the help gas are a factor in the trend of structural transition observed with methane.

Carbon Dioxide/Methylcyclohexane

The first system used for this study was the carbon dioxide/methylcyclohexane system. Phase equilibria data were collected over a pressure range of 1.7 MPa to 2.6 MPa and 275 K to 279 K, respectively. The data obtained from measurements on this system are listed in Table 6-5. These data are shown graphically on a pressure versus temperature plot in Figure 6-11.

Carbon Dioxide/2-Methylbutane

The second system used in this study involved carbon dioxide and 2-methylbutane. Phase equilibria data were collected over a pressure range of 1.5 MPa to 4.0 MPa and 275 K to 282 K, respectively. The data obtained from measurements on this system are listed in Table 6-6. These data are shown graphically on a pressure versus temperature plot in Figure 6-12.

Discussion

In examining the results of these two systems, the surprising observation was that there was only one region of bubble formation. Moreover, the noted region of bubble formation corresponds to the decomposition of carbon dioxide hydrates. Figure 6-13 shows a comparison plot of these experimental data from the two systems with phase equilibrium data for simple hydrates of carbon dioxide. These results indicate that, indeed, simple hydrates of carbon dioxide were formed and decomposed. Additionally, these results suggest there was not any structural transition from structure I to structure H upon hydrate decomposition. More specifically, structure H hydrates involving 2-methylbutane and methylcyclohexane did not form when carbon dioxide was used in place of methane as the help gas.

This unusual behavior has not been reported in the literature. A proposed explanation for this interesting activity could be rationalized by comparing the molecular dimensions of the two help gases with the molecular diameters of the two hydrate cavities which they occupy. From Table 2-2, the molecular diameters of methane and carbon dioxide are 4.36 Å and 5.12 Å, respectively. The two

Table 6-5. Experimental phase equilibria data for the carbon dioxide/methylcyclohexane system.

Temperature (K)	Pressure (MPa)
275.81	1.735
276.10	1.778
276.55	1.883
276.57	1.891
276.86	1.939
277.26	2.028
278.73	2.499
279.10	2.552

Table 6-6. Experimental phase equilibria data for the carbon dioxide/2-methylbutane system.

Temperature (K)	Pressure (MPa)
275.72	1.665
277.83	2.274
279.92	3.076
281.30	3.801

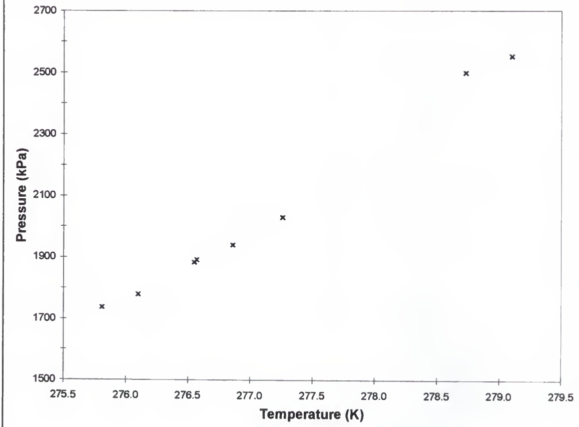

Figure 6-11. Plot of the experimental phase equilibria data for the carbon dioxide/methylcyclohexane system.

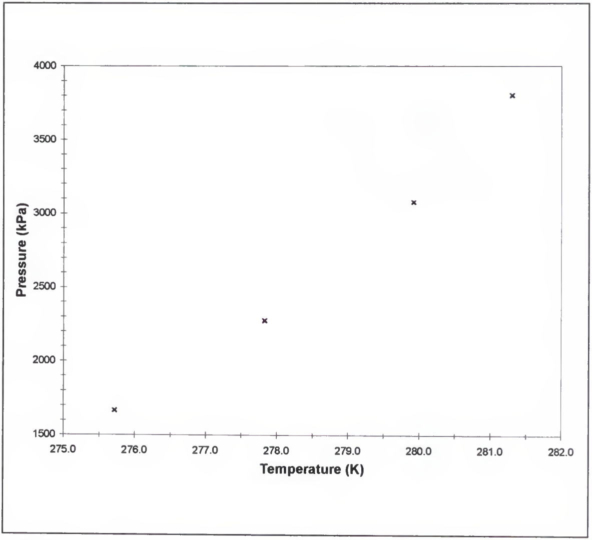

Figure 6-12. Plot of the experimental phase equilibria data for the carbon dioxide/2-methylbutane system.

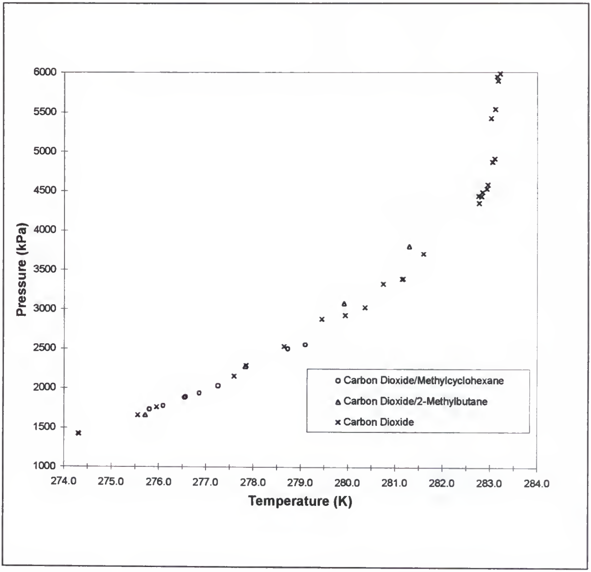

Figure 6-13. Comparison plot of the experimental data for the carbon dioxide/methylcyclohexane, carbon dioxide/ 2-methylbutane and carbon dioxide systems.

smaller cavities present in structure H are the 5^{12} and the $4^{3}5^{6}6^{3}$, with molecular diameters of 4.92 Å and 5.22 Å, respectively. The diameter ratio of methane to the 5^{12} cavity is 0.886 while the diameter ratio of methane to the $4^{3}5^{6}6^{3}$ cavity is 0.835. In comparison, the diameter ratio of carbon dioxide to the 5^{12} cavity is 1.041 and to the $4^{3}5^{6}6^{3}$ cavity is 0.981.

Researchers have found that a guest molecule can not fit into a cavity without distortion if its molecular diameter to cavity diameter ratio is above the upper bound ratio limit of about 1.0. Thus, for help gases used in the formation of structure H hydrates, the structural transition from structure I to structure H may be due to the additional stability gained by the help guest gas molecules occupying the 5^{12} and $4^{3}5^{6}6^{3}$ cavities. From this comparison, carbon dioxide appears to be too big to fit in the 5^{12} and $4^{3}5^{6}6^{3}$ cavities of structure H hydrates. Therefore, experimental results show only the formation of carbon dioxide hydrates and none of the 2-methylbutane or methylcyclohexane-containing structure H hydrates.

Methane/2,4-Pentanedione

The next system studied involved methane and the liquid 2,4-pentanedione. Phase equilibria data were collected over a pressure range of 4.0 MPa to 6.5 MPa and 275 K to 280 K, respectively. The data obtained from measurements on this system are listed in Table 6-7. These data are shown graphically on a pressure versus temperature plot in Figure 6-14.

For this system, only one region of bubble formation was seen. Additionally, the structural transition from structure I to structure H, as seen when methane was used with methylcyclohexane and 2-methylbutane, was completely absent. In fact, at a given temperature, the pressure required for the formation of the 2,4-pentanedione hydrate was about 23% higher than that required for the methane hydrate formation. This comparison is shown with a plot in Figure 6-15.

The approximate molecular diameters of the three liquid hydrocarbons methylcyclohexane, 2-methylbutane and 2,4-pentanedione are 8.6 Å, 7.8 Å and 8.5 Å, respectively. The diameter of the $5^{12}6^{8}$ cavity, the largest of the three cavities in structure H hydrates, is 8.53 Å. An approximate upper limit on the diameter of guests which can form structure H hydrates was determined to be 8.6 Å by Ripmeester.[18] Thus, it would be expected that all three compounds would form structure H hydrate.

Although structure H hydrate could be formed by a large number of guest molecules, size considerations alone were not sufficient for a molecule to be a suitable guest. Ripmeester determined, for example, that *trans*-2-butene and the methylbutenes, while they were of suitable sizes to fit

Table 6-7. Experimental phase equilibria data for the methane/2,4-pentanedione system.

Temperature (K)	Pressure (MPa)
275.57	4.088
276.19	4.421
276.75	4.657
276.85	4.764
277.82	5.281
278.49	5.555
279.06	5.932
279.58	6.159
279.97	6.414

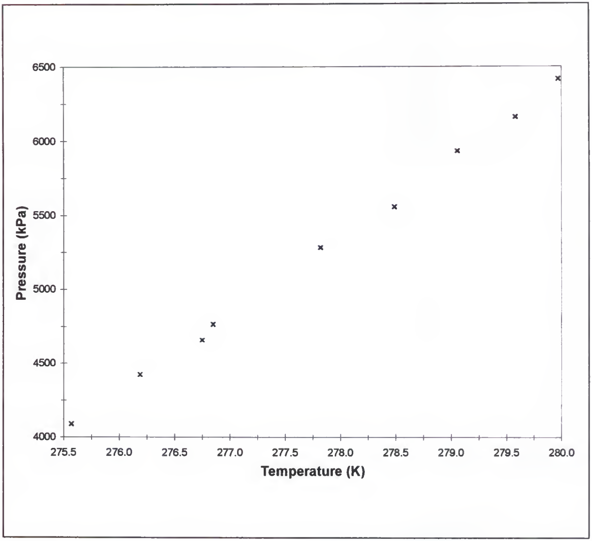

Figure 6-14. Plot of the experimental phase equilibria data for the methane/2,4-pentanedione system.

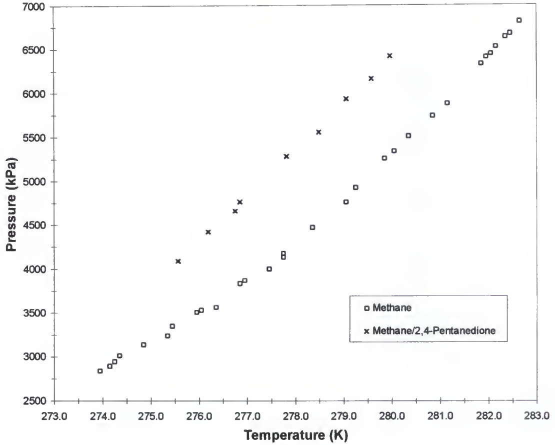

Figure 6-15. Comparison plot of the experimental data involving the methane/2,4-pentanedione system with the methane system.

in the $5^{12}6^{8}$ cavity, did not form any structure H hydrates. Efficient space filling of the cavity by the guest species to maximize van der Waals contact between the guest and the cage walls was an important factor. It should be pointed out that this space filling concept was not a factor for structure I and II hydrates, where with a few exceptions, all molecules of the appropriate sizes will stabilize the hydrate.

The results obtained in the study of the methane/2,4-pentanedione system could possibly be explained by looking at the structure of 2,4-pentanedione. This compound exists in the keto form as well as its enol tautomeric form.[54-56] In solution, the enol form of 2,4-pentanedione predominates, and this tautomeric form is known to exhibit intramolecular hydrogen bonding. Thus, the 2,4-pentanedione molecules may be of smaller size than earlier indicated. The molecular diameter of the enol form of 2,4-pentanedione, approximated using HYPERCHEM®, was about 8.2 Å, which is 0.3 Å smaller than its keto form.

The fact that the enol form of 2,4-pentanedione exhibits intramolecular hydrogen bonding, coupled with the high formation pressures required for hydrate formation, leads to the hypothesis that the compound possibly may be participating in hydrogen bonding with the framework of the hydrate crystal lattice. Moreover, the methane/2,4-pentanedione system perhaps could be forming a new hydrate structure. Naturally, more work needs to be done before any definite conclusions can be reached.

Recent experimental measurements have been reported in the literature for the hydrate-forming systems methane/acetone and methane/tetrahydrofuran (THF).[57-58] These studies showed the unexpected behavior of acetone and THF acting both as a hydrate promoter and hydrate inhibitor. At low concentrations, typically below 15% by weight, acetone and THF appear to behave as hydrate promoters, by lowering the pressures required for hydrate formation at a particular temperature. Moreover, at high concentrations, both acetone and THF appear to behave as hydrate inhibitors, by raising the pressures needed for hydrate formation at a certain temperature. The influence of acetone and THF on the hydrate formation process is not understood. It appears likely that 2,4-pentanedione may behave in a similar way. More experiments are necessary, particularly with varying weight percent of 2,4-pentanedione, in order to further explain the behavior of the methane/2,4-pentanedione system.

Enthalpy of Dissociation (ΔH_d) Determination

The process of hydrate decomposition is given by the simple expression:

$$\text{Hydrate} \leftrightarrow \text{Water} + \text{Gas} \qquad (6\text{-}2)$$

In cases where a second liquid phase does not occur, the most direct and accurate way of determining the dissociation enthalpy for the decomposition reaction shown above is to measure it calorimetrically.[46-48] Another way of obtaining the heat of dissociation is to estimate it through the use of thermodynamics and available phase equilibrium data. This method, valid for simple hydrates, is shown in some detail below.

Consider the closed system of constant volume at the hydrate decomposition point. Equations 6-3 and 6-4 show the physical reaction of the decomposition process.

$$\text{Hydrate} \leftrightarrow 1 \text{ mole } H_2O + x \text{ moles gas } (P,T) \qquad (6\text{-}3)$$

$$\text{Hydrate} \leftrightarrow 1 \text{ mole } H_2O + x \text{ moles gas } (P+dP,T+dT) \qquad (6\text{-}4)$$

The variable x represents the number of moles of gas per mole of water in the simple hydrate. There is great variation in the literature for values of x reported for methane hydrates, ranging from 0.135 to 0.174 (5.75 to 7.4 moles of water per mole of methane).[38,41,46-47] This is in accord with the non-stoichiometry of hydrates. The composition depends on the conditions under which the hydrate is formed and maintained. This behavior is believed to be typical for hydrates. For carbon dioxide hydrates, however, there is not any available data on the molar ratio of gas to water.

At the decomposition point, three phases exist in equilibrium; liquid water, gas and hydrate. The change in the Gibbs' free energy of the system can be expressed as,

$$d\Delta G = \Delta dG = d\tilde{G}_{H_2O} + x d\tilde{G}_{gas} - d\tilde{G}_{hyd} = 0 \qquad (6\text{-}5)$$

in which $\tilde{G}_{H_2O}$, $\tilde{G}_{gas}$ are the molar free energies of water, gas and $\tilde{G}_{hyd}$ is the molar free energy of hydrate per mole of water. Equation 6-5 can be expressed in a more useful form,

$$-\tilde{S}_{H_2O}dT - x\tilde{S}_{gas}dT + \tilde{S}_{hyd}dT + \tilde{V}_{H_2O}dP + x\tilde{V}_{gas}dP - \tilde{V}_{hyd}dP = 0 \qquad (6\text{-}6)$$

or,

$$\Delta V dP - \Delta S dT = 0 \qquad (6\text{-}7)$$

In equation 6-6, $\tilde{S}_{H_2O}$, $\tilde{S}_{gas}$, $\tilde{S}_{hyd}$ and $\tilde{V}_{H_2O}$, $\tilde{V}_{gas}$ and $\tilde{V}_{hyd}$ are the molar entropies and volumes of water, gas and hydrate according to the convention used above for Gibbs' free energy.

Rewriting equation 6-7 gives,

$$\frac{dP}{dT} = \frac{\Delta S}{\Delta V} = \frac{\Delta H}{T\Delta V} \qquad (6\text{-}8)$$

$$\frac{dP/P}{dT} = \frac{d\ln P}{dT} = \frac{\Delta H}{TP\Delta V} \qquad (6\text{-}9)$$

$$\frac{d\ln P}{dT} = \frac{\Delta H}{TP\left\{\left(\tilde{V}_{H_2O} - \tilde{V}_{hyd}\right) + x\tilde{V}_{gas}\right\}} \qquad (6\text{-}10)$$

$$\frac{d\ln P}{dT} = \frac{\Delta H}{RT^2}\left\{\frac{RT}{P\left(\tilde{V}_{H_2O} - \tilde{V}_{hyd} + x\tilde{V}_{gas}\right)}\right\} \qquad (6\text{-}11)$$

$$\frac{d\ \ln P}{dT} = \frac{\Delta H / RT^2}{\dfrac{P\left(\tilde{V}_{H_2O} - \tilde{V}_{hyd}\right)}{RT} + x\left(\dfrac{P\tilde{V}}{RT}\right)_{gas}} \tag{6-12}$$

The term $\left(\dfrac{P\tilde{V}}{RT}\right)_{gas}$ is the compressibility Z, which is well known for both methane and carbon dioxide over wide ranges of temperature and pressure. In terms of Z, equation 6-12 becomes,

$$\frac{d\ \ln P}{dT} = \frac{\Delta H / RT^2}{\dfrac{P\left(\tilde{V}_{H_2O} - \tilde{V}_{hyd}\right)}{RT} + xZ_{gas}} \tag{6-13}$$

Equation 6-13 can be rewritten to give a more familiar form,

$$\left(\frac{d\ \ln P}{d\left(\frac{1}{T}\right)}\right) = -\frac{\Delta H}{R}\ \frac{1}{\left[\dfrac{P\left(\tilde{V}_{H_2O} - \tilde{V}_{hyd}\right)}{RT} + xZ_{gas}\right]} \tag{6-14}$$

Using the experimental phase equilibria data, a plot of the logarithm of the hydrate decomposition pressure against the reciprocal temperature will give a straight line with slope m. The slope of this plot then can be used to approximate the heat of dissociation (ΔH_d) using the expression given below in equation 6-15.

$$\left(\frac{d\ \ln P}{d\left(\frac{1}{T}\right)}\right) = m = -\frac{\Delta H}{R}\,\frac{1}{\left[\frac{P\left(\tilde{V}_{H_2O} - \tilde{V}_{hyd}\right)}{RT} + xZ_{gas}\right]} \qquad (6\text{-}15)$$

The molar volume[49] of water is 18.0 cm^3 and $\tilde{V}_{hyd}$, the volume of the empty lattice of hydrate structure I per mole of water is 22.8 cm^3. The values of Z for methane and carbon dioxide can be obtained using the AGA8 equation of state.[50] As indicated earlier, x is the number of moles of gas per mole of water in the hydrate. The variables R, T and P have their usual meanings. Thus, experimental phase equilibria data can then be used to estimate ΔH_d at each of the hydrate decomposition temperature and pressure.

Calculations were carried out to determine values of ΔH_d using the phase equilibria data for the simple hydrates of methane and carbon dioxide. Recall that the unit crystal structure of SI has the formula $2M_1 \bullet 6M_2 \bullet 46H_2O$. In the methane system, a value of 0.166 (1 mole of gas for every 6 moles of water) was used for x, whereas a value of 0.130 was used for the carbon dioxide system. At 274.3 K, the heat of dissociation of methane hydrate was estimated to be 9.37 kJ/mol H_2O, whereas for carbon dioxide hydrate, this value was 9.18 kJ/mol H_2O.

Handa[46] reported a ΔH_d value of 54.19 kJ/mol hydrate for methane hydrates at 273.15 K. This value assumed the hydrate had the composition of $CH_4 \bullet 6H_2O$. For comparison purposes, using the composition of $CH_4 \bullet 6H_2O$, the ΔH_d value estimated from experimental data in this work corresponded to 56.22 kJ/mol of hydrate for methane. This comparison yielded a 3.7% difference in the value for ΔH_d of methane hydrates. Using a composition of $CO_2 \bullet 7.6H_2O$ leads to a value of 70.38 kJ/mol hydrate for carbon dioxide. Literature values for the dissociation enthalpy of CO_2 hydrates were not available for comparison.

CHAPTER 7
CONCLUSION AND RECOMMENDATIONS

A goal of this research was to develop a cell capable of stimulating hydrate growth and decomposition under appropriate temperatures and pressures. This goal was accomplished when the hydrate visual cell was designed, fabricated and initially tested using the methane/water system. Experimental phase equilibria data for several hydrate-forming systems were determined using the hydrate cell discussed in this document. For previously studied systems, these experimental results were in excellent agreement with those of other researchers.

Experimentally, the compact hydrate apparatus was placed under a microscope for observation during warming runs to determine the hydrate decomposition temperature and pressure. The microscope enabled close visual examination and video recording of the hydrate cell's contents as it was heated. This technique was capable of yielding definite visual confirmation of hydrate decomposition along with temperature and pressure information. The onset of hydrate decomposition was noted by the formation of microscopic gas bubbles. An increasing number of bubbles was observed to form as the decomposition temperature was reached and exceeded. The hydrate decomposition point was taken to be the temperature and pressure at which these microscopic gas bubbles first formed.

The current design of the apparatus puts a restraint on system pressure with an upper limit around 7.5 MPa. The temperature of 271 K appears to be the present temperature limit on cooling the cell. For greater versatility, the apparatus needs to be modified to operate at more extreme pressures and temperatures. These modifications would enable the study of the behavior of simple hydrates involving components such as argon or nitrogen, which form at pressures much higher than those required to form methane or carbon dioxide hydrates. Moreover, such changes would allow the cell to probe the phase equilibria behavior of hydrate-forming systems at pressure and temperature conditions similar to those found deep below the surface of the Earth.

As with any apparatus intended for extensive use, ultimately, there is a need for automation. The present work requires the constant monitoring of system temperature by the experimenter. Automated temperature control capability would be of great benefit, especially on heating runs, in order to provide a constant heating rate or to maintain constant temperature over a specified length of time.

For the investigation of structural transition from structure I to structure H, much more work needs to be done.

In particular, gases such as argon, nitrogen, ethane or xenon can be used in place of methane and carbon dioxide to examine further the effect of guest size on structural stability and structural transition. Moreover, different liquid hydrocarbons of various molecular diameters should be used as well. The cell shows excellent potential for determining the phase equilibria of any system of interest. Naturally, this technique and apparatus require additional confirmation from sources such as NMR and X-ray crystallography to definitely confirm any new hydrate structure formation.

APPENDIX A
COMPUTER PROGRAMS

Listed below are the source codes for the programs used in the data acquisition. The programs were written using ANSI C standard code language. The programs were written by the author. Program couple.c was used for data acquisition where the copper-constantan thermocouple was used. Program rtd.c was used for data acquisition when the miniature RTD was used.

Program couple.c

```
#include <stdio.h>
#include <stdlib.h>
#include <math.h>
#include <string.h>
#include <decl.h>          /* supplied with driver libraries */
#include <conio.h>
#include <time.h>
#include <graph.h>

#define cls()              _clearscreen(_GCLEARSCREEN)

FILE *stream;


double readT()
{
int i, probe;
double res;
char rstring[17];
    probe = ibfind("K195Temp");
    ibrd( probe, rstring, 17 );
    for(i=0; i<4; i++) rstring[i]=' ';
    rstring[16]=0x00;
    res=(double)atof(rstring);
    return (res);
}


double readP()
{
int i, probe;
double res;
char rstring[20];
    probe = ibfind("Beckman");
    ibrd( probe, rstring, 16 );
    res=(double)atof(rstring);
    return (res);
}


main()

{
clock_t ticksnow;
double Voltage, Press, t[2], ttrip;
double Pressure, Temperature;

    printf("Opening file\n");
    printf("Writing file c:\\vu\\data\\run1.dat\n\n");
    if((stream=fopen("c:\\vu\\data\\run1.dat", "w"))== NULL)
       perror( "OK, Error" );


    t[0]=0;
    ttrip=0.0;
    do
    {
      Voltage=readT();        /*gets thermocouple (voltage)*/
      Press=readP();          /*gets pressure (psi)*/
      ticksnow=clock();                   /*gets time*/
      t[1]=(double)ticksnow/CLK_TCK;      /*in seconds*/
      if(t[1]>ttrip)
     {
      Temperature=((25332*Voltage)-0.0396); /*volts to C*/

      Voltage = Voltage * 1000;

      Pressure = (Press+14.08)/1.0009; /* Pressure Calib. */

      printf("T= %.2f secs Voltage= %.4f mV Temp= %.1f C
               Pressure= %.1f psi\n", t[1]-t[0], Voltage,
               Temperature, Pressure);
      fprintf(stream, "%.2f %.2f %.1f %.1f %.4f\n", t[1],
               t[1]/60.0, Temperature, Pressure, Voltage);
      ttrip=ttrip+2;
     }
    }

    while (!kbhit());

    printf("Closing file\n");
    fclose(stream);

}
```

Program rtd.c

```
#include <stdio.h>
#include <stdlib.h>
#include <math.h>
#include <string.h>
#include <decl.h>          /* supplied with driver libraries */
#include <conio.h>
#include <time.h>
#include <graph.h>

#define cls()              _clearscreen(_GCLEARSCREEN)

#define alpha  0.00385
#define delta  1.502
#define Ro  100.00

FILE *stream;



double readT()
{
int i, probe;
double res;
char rstring[17];
    probe = ibfind("K195Temp");
    ibrd( probe, rstring, 17 );
    for(i=0; i<4; i++) rstring[i]=' ';
    rstring[16]=0x00;
    res=(double)atof(rstring);
    return (res);
}
```

```
double readP()
{
int i, probe;
double res;
char rstring[20];
    probe = ibfind("Beckman");
    ibrd( probe, rstring, 16 );
    res=(double)atof(rstring);
    return (res);
}


main()

{
clock_t ticksnow;
double Rt, Press, t[2], ttrip;
double A, B, Pressure, Temperature;

    printf("Opening file\n");
    printf("Writing file c:\\vu\\data\\run1.dat\n\n");
    if((stream=fopen("c:\\vu\\data\\run1.dat", "w"))== NULL)
       perror( "OK, Error" );

    A = alpha * (1 + (delta/100));
    B = -(alpha * delta * 0.0001);

    t[0]=0;
    ttrip=0.0;
    do
    {
      Rt = readT() - 0.160;  /*leads resistance subtracted*/
      Press = readP();       /*gets pressure (psi)*/
      ticksnow=clock();              /*gets time*/
      t[1]=(double)ticksnow/CLK_TCK; /*in seconds*/
      if(t[1]>ttrip)
     {
      Temperature = (-A + sqrt((A*A)-(4*B)*(1-(Rt/Ro)))) /
                         (2*B);          /*resistance to C*/

      Pressure = (Press + 14.08) / 1.0009;  /*Press Calib*/

      printf("T = %.2f secs   R = %.3f Ohms  Temp = %.2f C
               Press = %.1f psi\n", t[1]-t[0], Rt,
               Temperature, Pressure);
      fprintf(stream, "%.2f %.2f %.2f %.1f %.3f\n", t[1],
              t[1]/60.0, Temperature, Pressure, Rt);
      ttrip=ttrip+2;
     }
    }

    while (!kbhit());

    printf("Closing file\n");
    fclose(stream);

}
```

APPENDIX B
ICE FORMATION

Condensation and ice formation on the external window surface of the hydrate cell was a recurring problem in the developmental stages of this research. The formation of ice prevented the visual examination of the cell's contents. Figure B shows a typical image seen under the microscope when such a problem occurred. Ice formation was eliminated by flowing a stream of nitrogen gas over the window surface. This provided an unobstructed view of the hydrate cell's contents. Thus, visual detection of the formation of microscopic bubbles upon hydrate decomposition was then possible.

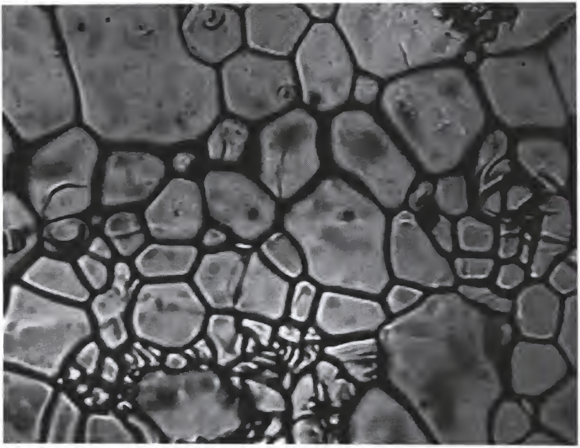

Figure B. Image of ice formation on the outside surface of the sapphire window.

APPENDIX C
TEMPERATURE CONTROL

Temperature control of the hydrate cell was possible by controlling the temperature of a solution of diethylene glycol/water. This coolant was allowed to circulate through the insulated brass block which was used to house the hydrate cell. Initial concern was with the design and whether it would provide adequate temperature control in the stepwise cooling or warming processes. To ensure the system under study had reached an equilibrated state, initial experiments were carried out to determine the time necessary for the cell to reach temperature equilibration after a set-point was fixed. In all these experiments, system temperature was recorded as a function of time.

Figure C-1 is an example of one such run where the system was cooled from 275.5 K to 271.5 K. Equilibration, in this process, required approximately 20 minutes and the cell's temperature was observed to fluctuate around 271.5 K. Figure C-2 shows the plot of the cell's temperature versus time where the coolant's temperature was held constant. The plot indicates the cooling block's capability of maintaining cell temperatures with an average temperature of 271.61 K with a standard deviation of ± 0.02 K over the 70 minute time period.

Rapid temperature equilibration on warming runs was especially critical for the determination of hydrate phase equilibria data. Figures C-3 and C-4 show the plots of cell temperature as a function of time to illustrate the approximate time needed for temperature equilibrium on heating runs. In Figure C-3, the temperature was raised by 1.0 K. Figure C-4 shows the activity when the cell was raised by 0.1 K. In either case, the time required for temperature equilibration was approximately 10 minutes. These results demonstrate the cooling block's ability to provide rapid temperature equilibration and maintain temperature control during heating. The time of ten minutes was used as the minimum period to wait between successive temperature increments in order for sufficient temperature equilibration to occur.

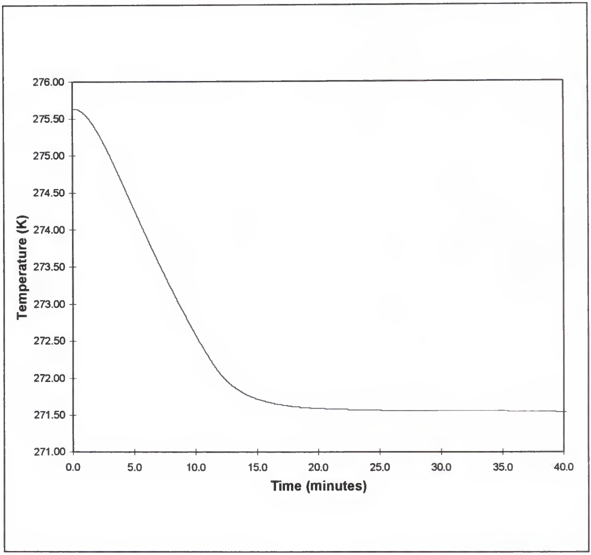

Figure C-1. Plot of cell temperature versus time under cooling conditions.

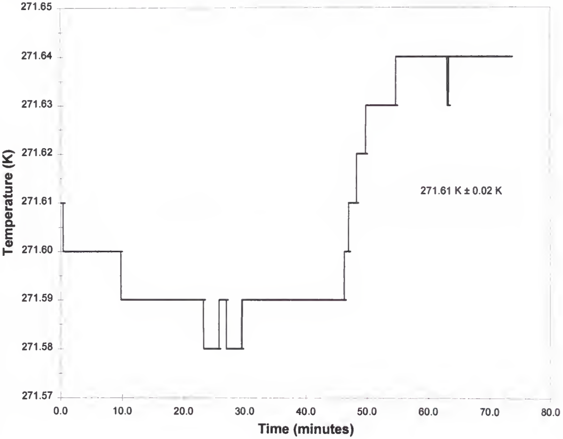

Figure C-2. Plot of cell temperature versus time under isothermal control.

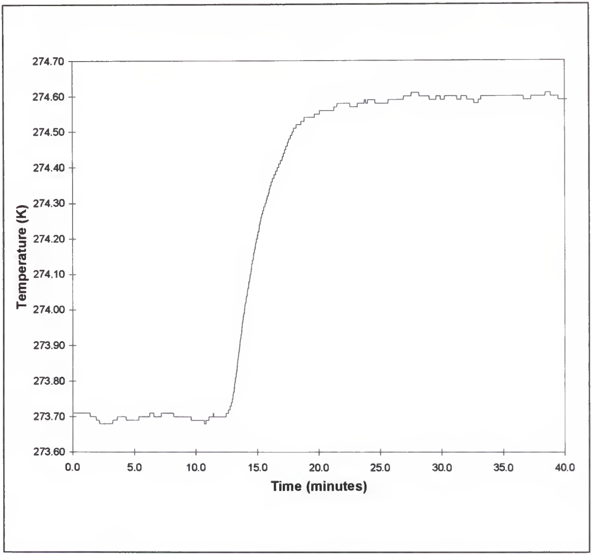

Figure C-3. Cell temperature versus time plot of a system undergoing a programmed 1.0 K temperature change.

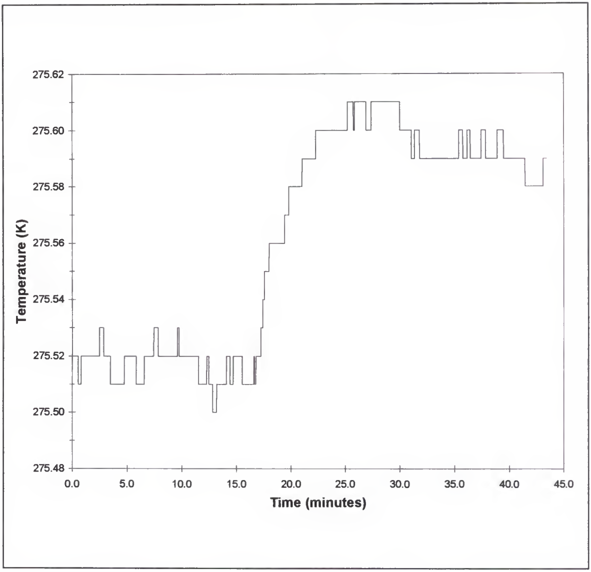

Figure C-4. Cell temperature versus time plot of a system undergoing a programmed 0.1 K temperature change.

REFERENCES

1. Davy H., Phil. Trans. Roy. Soc. London, **101**, 1, 1811.

2. Faraday M., Phil. Trans. Roy. Soc. London, **113**, 160, 1823.

3. Hammerschmidt E.G., Ind. Eng. Chem., **26** (8), 851, 1934.

4. Sloan E.D. Jr., "Clathrate Hydrates of Natural Gases," Marcel Dekker Inc., New York, 1990.

5. Kvenvolden K.A., Chemical Geology, **71**, 41, 1988.

6. Makogon Y.F., Natural Gas Hydrates: The State of Study in the USSR and Perspectives for Its Use, paper presented at the Third Chemical Congress of North America, Toronto, Canada, June 5-10, 1988.

7. Vysniauskas A. and P.R. Bishnoi, Chemical Engineering Science, **38**, 1061, 1983.

8. Englezos P., Ind. Eng. Chem. Res., **32**, 1251, 1993.

9. Sloan E.D. Jr. and F. Fleyfel, AIChE Journal, **37**, 1281, 1991.

10. Mehta A.P. and E.D. Sloan Jr., J. Chem. Eng. Data, **38**, 580, 1993.

11. Christansen R.L. and E.D. Sloan Jr., Annals of New York Academy of Sciences, **715**, 168, 1994.

12. McMullan R.K. and G.A. Jeffrey, J. Chem. Phys., **42**, 2725, 1965.

13. Mak T.C.W. and R.K. McMullan, J. Chem. Phys., **42**, 2732, 1965.

14. Ripmeester J.A., Tse J.S., Ratcliffe C.I. and B.M. Powell, Nature, **325**, 135, 1987.

15. Lederhos J.P., Mehta A.P., Nyberg, G.B., Warn K.J., and E.D. Sloan, AIChE Journal, **38**, 1045, 1992.

16. Davidson D.W., Can. J. Chem., **49**, 1224, 1971.

17. Ripmeester J.A. and D.W. Davidson, J. Mol. Struct., **75**, 67, 1981.

18. Glew D.N., Nature, **184**, 545, 1959.

19. Ripmeester J.A. and C.I. Ratcliffe, J. Phys. Chem., **94** (25), 8773, 1990.

20. Mehta A.P. and E.D. Sloan Jr., J. Chem. Eng. Data, **39**, 887, 1994.

21. Ng H. -J. and D.B. Robinson, Fluid Phase Equilibria, **21**, 145, 1985.

22. Ng H. -J., Chen C. -J. and T. Saeterstad, Fluid Phase Equilibria, **36**, 99, 1987.

23. Holder G.D., Zetts S.P. and N. Pradhan, Rev. Chem. Eng., **5**, 1, 1988.

24. Ng H. -J. and D.B. Robinson, Ind. Eng. Chem. Fund., 15, **293**, 1976.

25. Dholabhai P.D., Englezos P., Kalogerakis N. and P.R. Bishnoi, Can. J. Chem. Eng., **69**, 800, 1991.

26. Englezos P., Kalogerakis N., Dholabhai P.D. and P.R. Bishnoi, Chem. Eng. Sci., **42**, 2647, 1987.

27. Englezos P., Kalogerakis N., Dholabhai P.D. and P.R. Bishnoi, Chem. Eng. Sci., **42**, 2659, 1987.

28. Natarajan V., Bishnoi P.R. and N. Kalogerakis, Chem. Eng. Sci., **49**, 2075, 1994.

29. Bishnoi P.R., Natarajan V. and N. Kalogerakis, Annals of New York Academy of Sciences, **715**, 311, 1994.

30. Bishnoi P.R. and V. Natarajan, Fluid Phase Equilibria, **117**, 168, 1996.

31. Fleyfel F., Song K.Y., Kook A., Martin R. and R. Kobayashi, Annals of New York Academy of Sciences, **715**, 212, 1994.

32. Baez A.L. and P. Clancy, Annals of New York Academy of Sciences, **715**, 177, 1994.

33. Plummer P.L.M. and T.S. Chen, J. Phys. Chem., **87**, 4190, 1983.

34. Plummer P.L.M. and T.S. Chen, J. Chem. Phys., **86**, 7149, 1987.

35. Schroeter J.P., Kobayashi R. and M.A. Hildebrand, Ind. Eng. Chem. Fundam., **22**, 361, 1983.

36. Nerheim A.R., Svartaas T.M. and E.J. Samuelsen, Proceedings of The Second International Offshore and Polar Engineering Conference, San Francisco, U.S.A., 1992.

37. Adisasmito S., Frank R.J. and E.D. Sloan Jr., J. Chem. Eng. Data, **36**, 68-71, 1991.

38. Deaton W.M. and E.M. Frost Jr., U.S. Bureau of Mines Monograph, **8**, 1946.

39. Jhaveri J. and D.B. Robinson, Can. J. Chem. Eng., **43**, 75, 1965.

40. Verma V.K., Gas Hydrates from Liquid Hydrocarbon-Water Systems Ph.D. Thesis, University of Michigan, 1974, Univ. Microfilms No. 75-10, 324, Ann Arbor, MI.

41. de Roo J.L., Peters C.J., Lichtenthaler R.N. and G.A.M. Diepen, AIChE J., **29**, 651, 1983.

42. Thakore J.L. and G.D. Holder, Ind. Eng. Chem. Res., **26**, 462, 1987.

43. Robinson D.B. and B.R. Mehta, J. Can. Petr. Tech., **10**, 33, 1971.

44. Larson S.D., Phase Studies of the Two-Component Carbon Dioxide-Water System, Involving the Carbon Dioxide Hydrate, Ph.D. Thesis, University of Illinois, 1955.

45. Ng H. -J. and D.B. Robinson, Fluid Phase Equilibria, **21**, 145, 1985.

46. Handa Y.P., J. Chem. Thermo., **18**, 915, 1986.

47. Handa Y.P., J. Chem. Thermo., **18**, 891, 1986.

48. Rueff R.M., Sloan E.D., Jr., and V.F. Yesavage, AIChE Journal, **34**, 1468, 1988.

49. Barrer R.M. and W.I. Stuart, Proc. Roy. Soc. (London) A, No. 1233, **243**, 172, 1957.

50. Starling K.E. editor, AGA8 "Compressibility and supercompressibility for natural gas and other hydrocarbon gases", AGA Transmission measurement committee report number 8 (AGA8), American Gas Association, 1986.

51. Thomas M. and E. Behar, Proceedings of the 73rd Gas Processors Association Annual Convention, 100, 1994.

52. Hutz U. and P. Englezos, Fluid Phase Equilibria, **117**, 178, 1996.

53. Mehta A.P. and E.D. Sloan Jr., Proceedings of the 75th Gas Processors Association Annual Convention, 27, 1996.

54. Rogers M.T. and J.L. Burdett, Can. J. Chem., **43**, 1516, 1965.

55. Burdett J.L. and M.T. Rogers, J. Amer. Chem. Soc., **86**, 2105, 1964.

56. Drexler E.J. and K.W. Field, J. Chem. Educ., **53**, 393, 1976.

57. Ng H. -J. and D.B. Robinson, Annals of New York Academy of Sciences, **715**, 450, 1994.

58. Saito Y., Kawasaki T., Kondo T. and R. Hiraoka, 2nd International Conference on Natural Gas Hydrates, June 2-6, 1996, Toulouse, France, 459.

BIOGRAPHICAL SKETCH

Vu H.Q. Thieu was born on October 11, 1968, in Saigon, Vietnam. In October of 1979, he managed to escape war-torn and Communist-controlled Vietnam with his older brother. He arrived in St. Cloud, Minnesota, in late February of 1980. Under the guidance and support of his uncle, he attended South Junior High School and Technical High School. In June of 1987, he graduated from high school and immediately began his collegiate education at St. John's University in Collegeville, Minnesota. His chemistry research experience started there under the directions of Dr. Richard Jochman.

After enduring four more bitter-cold Minnesota winters, the author received his Bachelor of Science degree in chemistry from St. John's University in May of 1991. Yearning for warmer weather, he immediately selected the University of Florida for graduate school in chemistry. In late 1991, he joined the research laboratory of Dr. Samuel Colgate in the Physical Chemistry Division. His principle areas of research included developing the instrumentation and methods for studying clathrate hydrate phase equilibria. Upon completing the requirements for the doctoral thesis, he will join the laboratory of Dr. E. Dendy Sloan, Jr. of the

Colorado School of Mines to continue studying the chemistry of clathrate hydrates.

I certify that I have read this study and that in my opinion it conforms to acceptable standards of scholarly presentation and is fully adequate, in scope and quality, as a dissertation for the degree of Doctor of Philosophy.

Samuel O. Colgate

Samuel O. Colgate, Chair
Professor of Chemistry

I certify that I have read this study and that in my opinion it conforms to acceptable standards of scholarly presentation and is fully adequate, in scope and quality, as a dissertation for the degree of Doctor of Philosophy.

John R. Eyler

John R. Eyler
Professor of Chemistry

I certify that I have read this study and that in my opinion it conforms to acceptable standards of scholarly presentation and is fully adequate, in scope and quality, as a dissertation for the degree of Doctor of Philosophy.

Luis M Muga

Luis M. Muga
Professor of Chemistry

I certify that I have read this study and that in my opinion it conforms to acceptable standards of scholarly presentation and is fully adequate, in scope and quality, as a dissertation for the degree of Doctor of Philosophy.

James Boncella

James Boncella
Associate Professor of Chemistry

I certify that I have read this study and that in my opinion it conforms to acceptable standards of scholarly presentation and is fully adequate, in scope and quality, as a dissertation for the degree of Doctor of Philosophy.

Paul Ehrlich

Paul Ehrlich
Professor of Mathematics

This dissertation was submitted to the Graduate Faculty of the Department of Chemistry in the College of Liberal Arts and Sciences and to the Graduate School and was accepted as partial fulfillment of the requirements for the degree of Doctor of Philosophy.

May 1997

Dean, Graduate School